Cloud Ice: A Climate Model Challenge With Signs and Expectations of Progress

Duane Waliser/JPL, Frank Li/JPL, C. Woods/JPL,
R. Austin/CSU, J. Bacmeister/GSFC, J. Chern/GSFC, A. Del Genio/GISS, J. Jiang/JPL,
Z. Kuang/Harvard, H. Meng/NOAA, P. Minnis/Langley, S. Platnick/GSFC,
W.B. Rossow/CCNY/CUNY, G. Stephens/CSU, S. Sun-Mack/Langley, W.K. Tao/GSFC,
A. Tompkins/ECMWF, D. Vane/JPL, C. Walker/Harvard, D. Wu/JPL,

Submitted to
CloudSat Special Section Of JGR
February 22, 2008

Abstract

Present-day shortcomings in the representation of upper-tropospheric ice clouds in general circulation models (GCMs) lead to errors in weather and climate forecasts as well as account for a principal source of uncertainty in climate change projections. An ongoing challenge in rectifying these shortcomings has been the availability of adequate, high-quality, global observations targeting ice clouds and related precipitating hydrometeors. In addition, the inadequacy of the modeled physics and the often-disjointed nature between model representation and the characteristics of the observed values have hampered GCM development and validation efforts from making effective use of the observations that have been available. Thus, even though parameterizations in GCMs accounting for cloud ice processes have, in some cases, become more sophisticated in recent years, this development has largely occurred independently of the global scale observations. With the relatively recent addition of satellite-derived products from Aura/MLS and CloudSat, there are now considerably more resources with new and unique capabilities to evaluate GCMs. In this article, we illustrate the shortcomings evident in model

representations of cloud ice through a comparison of the simulations assessed in the IPCC Fourth Assessment Report, briefly discuss the range of global observational resources that are available, and describe the essential components of the model parameterizations that characterize their "cloud" ice and related fields. Using this information as background, we discuss some of the main considerations and cautions that must be taken into account in making model-data comparisons related to cloud ice, illustrate present progress and uncertainties in applying satellite cloud ice - namely from MLS and CloudSat - to model diagnosis, show some indications of model improvements, and finally discuss a number of remaining questions and suggestions for pathways forward.

Corresponding Author: Duane.Waliser@jpl.nasa.gov

1. Introduction

Upper tropospheric ice clouds that cover large spatial scales and persist in time strongly influence global climate through their effects on the Earth's radiation budget [*Liou*, 1976; *Hartmann and Short*, 1980; *Ramanathan et al.*, 1989; *Ramanathan and Collins*, 1991; *Randall and Tjemkes*, 1991; *Chen et al.*, 2000]. Many studies have pointed out that these clouds have influences through both their greenhouse and solar albedo effects with their relative influence depending strongly on their height, thickness, and optical and microphysical properties [*Stephens et al.*, 1981; *Hartmann and Doelling*, 1991; *Fu and Liou*, 1992; *Hartmann et al.*, 1992; *Kiehl*, 1994; *Miller*, 1997]. Deep convective clouds – which account for a very small fraction of cloud area – contain considerable contributions from ice as well as other frozen hydrometeors [*Krueger et al.*, 1995; *Rossow and Schiffer*, 1999; *Del Genio and Kovari*, 2002]. They play a crucial role in both weather and climate through vertical mixing and precipitation/latent heating, as well as through their connection to other larger-scale ice clouds such as precipitating anvil and non-precipitation cirrus clouds [e.g., *Luo and Rossow*, 2004]. Characterizations of ice cloud properties have been made using satellites [*Minnis et al.*, 1993; *Liao et al.*, 1995b; a; *Jin et al.*, 1996; *Rossow and Schiffer*, 1999; *Stubenrauch et al.*, 1999; *Wylie and Wang*, 1999; *Li et al.*, 2005] as well as in situ methods [*McFarquhar and Heymsfield*, 1996; *McFarquhar et al.*, 2000]. Such data and analyses have improved our understanding of ice cloud processes, and guided the directions for developing improved parameterizations of ice cloud microphysics. However, measurements of these ice clouds are still difficult to obtain due to the challenges involved in remotely sensing ice water content (IWC) and its vertical profile – including complications associated with multi-level clouds, mixed-phases and multiple hydrometeor types, the uncertainty in classifying ice particle size and shape for remote retrievals, the relatively small

time and space scales associated with deep convection, and the large dynamic range of cloud-related ice that exists when considering both sub-visible cirrus and the tops/interiors of deep convective clouds. Together, these measurement difficulties make it a challenge to characterize and understand the mechanisms of ice cloud formation and dissipation [*Liou*, 1975; *Liou and Ou*, 1989; *Wylie and Wang*, 1997; *Rossow and Schiffer*, 1999; *Luo and Rossow*, 2004; *Soden*, 2004; *Soden et al.*, 2004; *Wu et al.*, 2005; *Liu et al.*, 2007].

The importance of obtaining a more comprehensive understanding and improved capability for modeling upper-tropospheric ice clouds cannot be underestimated as "cloud feedbacks remain the largest source of uncertainty" in determining Earth's equilibrium climate sensitivity, specifically to a doubling of carbon dioxide [*IPCC*, 2007]. Some evidence for this uncertainty is given in Figure 1 that shows model-to-model comparisons of four different physical climate quantities, including cloud ice water path (IWP). While it is understood that models exhibit significant systematic spatial-temporal biases with respect to quantities such as precipitation, water vapor and clouds, their depiction of the global-averaged values is quite good. This stems from the fact that these quantities have had relatively robust long-standing observational constraints [*Arkin and Ardanuy*, 1989; *Rossow and Schiffer*, 1991; *Stephens et al.*, 1994; *Xie and Arkin*, 1997] as well as indirect measurement constraints via top of the atmosphere radiation measurements [*Gruber and Krueger*, 1984; *Kyle et al.*, 1993; *Smith et al.*, 1993]. In contrast, robust global (or globally representative in-situ) observations of cloud ice, particularly vertically-resolved values have not been available. Despite significant efforts to derive even IWP measurements from passive and nadir-viewing techniques, the large optical thicknesses, multi-layer structure and mixed-phase nature of many clouds makes the estimates from these techniques very uncertain [*Stephens et al.*, 2002; *Wu et al.*, 2006]. The sparse sampling of in-

situ observations and poor probing capabilities of nadir-viewing passive satellite IWC/IWP measuring techniques are highlighted in the schematic of Figure 2 in the context of the complexities of a precipitating and/or multi-layer cloud system. The ramifications of this poor constraint for cloud ice, even IWP, are evident in the much larger model-to-model disagreement for globally-averaged cloud ice shown in Figure 1. There is a *factor of 20* difference between the largest and smallest values, and even when the two largest outliers are removed, there is still a factor of about 6 between the largest and smallest values. As expected, these differences are exacerbated when considering the spatial patterns of the time-mean values shown in Figure 3; in some regions up to nearly two orders of magnitude. For a quantity as fundamental and relatively unambiguous as cloud ice mass, one that also has significant import within the context of climate change and its associated model projection uncertainties, it is critical that this level of model uncertainty be reduced.

Fortunately, there are new observational resources recently established that can be expected to lead to considerable reduction in the uncertainties associated with model representations of upper-tropospheric cloud ice. Specifically, these include the Microwave Limb Sounder (MLS) on the Earth Observing System (EOS) Aura satellite, and the CloudSat and CALIPSO satellite missions, all of which fly in formation in what is referred to as the A-Train [*Stephens et al.*, 2002]. Based on radar and limb-sounding techniques (see Figure 2), these new satellite measurements provide a considerable leap forward in terms of the information gathered regarding upper-tropospheric cloud ice water content as well as other macrophysical and microphysical properties. In this article, we briefly describe the current state of GCM representations of cloud ice and their associated uncertainties, the nature of the new observational resources for constraining cloud ice values in GCMs, the challenges in making

well-posed model-data comparisons, and prospects for near-term improvements in model representations. In section 2, we describe the satellite observations of IWP and IWC that are discussed in the article, with an indication of the relative strengths and weaknesses of the different retrieval methodologies and sensitivities. In section 3, we briefly describe the model resources that are examined and provide a rudimentary description of the various levels of complexity regarding model treatments of cloud ice. For both IWP and IWC, and for both the observations and the models, it is more or less understood that "ice" represents all frozen hydrometeors, which can include cloud ice – which is typically suspended or "floating", and ice mass precipitating forms such as snow and graupel. However, such distinctions are often not clearly made or are fuzzy, and a principle focus of this article is to help articulate where and how such distinctions are made and matter for model-data comparisons. In section 4, we present the results of the model data comparisons, with discussions regarding sampling, sensitivity, model representation, etc. In section 5, we conclude with a summary and discuss needs regarding future space-based retrievals and directions for model diagnosis and improvement.

2. Satellite Observations

In this section, we describe the satellite observations that are illustrated and discussed in this paper. To highlight a critical difference in capabilities, the observations are categorized as either passive nadir-viewing or radar/limb sounding. This distinction conveys a sense of their capabilities to account for vertical structure, namely in terms of being able to deal *less* ambiguously with multiple cloud levels and/or mixed-phase clouds. This leads to a pragmatic distinction of whether the satellite retrieval provides an estimate of (column-integrated) ice water path (IWP; gm m^{-2}) and/or has the capability to provide an estimate of (vertically-resolved) ice water content (IWC; mg m^{-3}). Given that this study mainly focuses on the new capabilities and

the associated uncertainties of the CloudSat and MLS retrievals, more details are provided regarding their methods and products. The passive nadir-viewing products are only referenced briefly and therefore the discussion below only provides highlights with many details left to the referenced literature.

a) Passive Nadir-Viewing

i) ISCCP

The International Satellite Cloud Climatology Project (ISCCP) provides an estimate of ice cloud water path (IWP) values based on measurements in the visible (VIS; 0.6 μm) and "window" infrared (IR; 11 μm). Because VIS measurements are used, results are obtained only in daytime (at 3 hr intervals) but are global except for the portions of the polar regions. The intrinsic resolution of the radiance measurements is determined by the pixel (field-of-view) size, about 5 km, and the sampling interval of about 30 km. After identifying cloud pixels, the cloud visible optical thickness (J) and cloud top temperature (T_C) are retrieved from the VIS and IR employing a radiative transfer model. The cloud top temperature is corrected for the transmission of IR radiation from below based on the values of J, the surface temperature (T_S) and the atmospheric temperature and humidity profile. The retrieval of J is based on one of two microphysical models, one for liquid and one for ice clouds. The phase of the cloud is determined by the value of T_C; if $T_C < 260$ K, the whole cloud is assumed to be an ice cloud. The microphysical model for ice clouds assumes a fractal particle shape with an aspect ratio of unity and an effective radius (r_E) = 30 μm and a size distribution variance of 0.1. Thus, the value of IWP can be determined from product of J, r_E and a coefficient that relates geometric cross section to volume for the assumed particle shape: for ice clouds in the ISCCP dataset, IWP (gm m^{-2}) = 10.05 J. For

additional details and discussions of uncertainties, see Rossow and Gardner [1993], Rossow and Schiffer [1999], Lin and Rossow [1996], Jin and Rossow [1997] and Han et al. [1999]. Annual mean ISCCP IWP values are shown in Figure 4.

ii) NOAA/NESDIS – AMSU-B/MHS

The NOAA/NESDIS IWP algorithm uses the measurements from the Advanced Microwave Sounding Unit – B (AMSU-B) and the Microwave Humidity Sounder (MHS) instruments to simultaneously retrieve IWP and ice particle effective diameter, D_e [*Zhao and Weng*, 2002; *Ferraro et al.*, 2005], through characterizations of the scattering properties of ice cloud. The first step of the retrieval is to derive D_e from a regression relation with the scattering parameter ratio of 89 GHz and 150 GHz. The relation was established using simulated data from a radiative transfer model. Then IWP is computed from the retrieved D_e and the scattering parameter of either 89 GHz or 150 GHz depending on the size of D_e. The retrieval can be done in all-weather conditions, during day or night, and has relatively high temporal coverage with up to 10 measurements per day owing to the five Polar Orbiting Environmental Satellites (POES) satellites (NOAA-15, -16, -17, -18, and MetOp-A). The NOAA IWP annual mean is shown in Figure 4. Its low bias relative to the other products shown is possibly due to two main reasons: scene screening criteria, which may bias the result, and insensitivity to small ice particles - in this case, less than 0.4 mm in size which is fairly large for many suspended cloud ice particles. The main screening criteria are that the scene be free of snow cover, and the brightness temperature at 89 GHz is higher than 150 GHz (due to the fact that the depression of brightness temperature increases with frequency from the scattering effect when atmospheric ice is present).

iii) CERES - MODIS

To determine IWP, the Clouds and the Earth's Radiant Energy System (CERES) algorithms [*Wielicki et al.*, 1998] first explicitly classify each 1-km Moderate Resolution Imaging Spectroradiometer (MODIS) cloudy pixel as ice or water based on the cloud temperature and the goodness of the match between the observed spectral radiances at three wavelengths and model calculations of the radiances using several different ice and water particle sizes [*Minnis et al.*, 1995; *Minnis and al.*, 2007]. The models use a set of hexagonal ice column distributions to represent ice cloud particles [*Minnis et al.*, 1998]. IWP is computed as a function of the product of the retrieved effective ice crystal size and optical depth for each pixel. Optical depth is limited to a maximum of 128 in the current CERES editions. The retrieval assumes that the entire cloud column is composed of ice. Although good agreement is found between ground-based cloud radar and the CERES retrievals of IWP for relatively thin cirrus clouds (optical depths < 4) with no underlying water clouds [*Mace et al.*, 2005], validation of IWP for thick clouds has not yet been performed, primarily due to a lack of reference data. Few ice clouds with optical depths less than 0.3 are detected by the CERES analysis [e.g., *Chiriaco et al.*, 2007], and while such clouds account for a significant portion of the ice-cloud cover, they contribute very little to the global IWP. More significant is the impact of multi-layered clouds on the IWP retrievals. *Huang et al.* [2006] and *Minnis et al.* [2007] showed that the assumption of the entire cloud column as ice leads to overestimates in IWP of roughly 50% in multi-layered cloud systems. Thus, if one assumes that half of all ice clouds overlap liquid clouds, then global estimates of IWP from passive visible, infrared, and near-infrared measurements are likely to be overestimated by around 25%. The data illustrated in Figure 4 use averages of IWP derived using Terra MODIS data taken for solar zenith angles less than 82°. The means are multiplied by the average ice

cloud fraction for each region to obtain all-sky IWP. In non-polar regions, the results correspond to 1030 LT.

iv) MODIS

The MODIS cloud optical and microphysical retrievals [*Platnick et al.*, 2003] are part of the archived MOD06 and MYD06 products (for Terra and Aqua MODIS, respectively) and use techniques similar to the CERES algorithm, though there are some differences, including the methods and data used for cloud masking [*Ackerman et al.*, 2008; *Frey et al.*, 2008, see also documentation at modis-atmos.gsfc.nasa.gov/products_C005update.html]. Determination of the thermodynamic phase of the cloud water uses a combination of infrared and shortwave infrared (SWIR) spectral tests [*King et al.*, 2004]. The ice cloud models used for the retrievals are based on in situ observations from a variety of cloud measuring campaigns and include size distributions with varying habit combinations as a function of size [*Baum et al.*, 2005]. The MODIS retrievals have been compared with the ground-based studies of Mace et al. [2005] and successful retrievals for ice clouds with optical thicknesses less than about 0.7 were less frequent than for CERES-MODIS however retrieval uncertainties in that range can be quite large. The ground-based and aircraft studies of Chiriaco et al. [2007] found similar conclusions. Figure 4 shows the mean global IWP from Aqua MODIS (generated from monthly Level-3 [*King et al.*, 2003] files and weighted by the ice cloud fraction to provide all-sky means. In the Level-3 product, monthly aggregations are derived from daily aggregations that include pixels from all orbits that contribute to the 1^{o} grid box, i.e., a true daily average and not an instantaneous one, though differences only occur poleward of about 30° due to the MODIS swath and become more significant in polar regions. A multilayer flag is generated in the processing but was not used to exclude pixels in the IWP values presented here.

b) Vertically-Resolving: Radar and Limb Sounding

i) MLS

The MLS onboard the Aura satellite, operational since August 2004, has five radiometers measuring microwave emissions from the Earth's atmosphere in a limb-scanning configuration to retrieve chemical composition, water vapor, temperature and cloud ice. The retrieved parameters consist of vertical profiles on fixed pressure surfaces having near-global (82°N-82°S) coverage. In formation with the rest of the so-called A-Train constellation of satellites, Aura has equatorial crossing times of approximately 1:30am and 1:30pm. The retrievals for IWC are provided at 100, 147, 215 and 316 hPa, where the latter is still experimental. Below about 250 hPa, contributions from mixed-phase clouds and stronger water vapor emission, particularly in the tropics, make the retrievals more uncertain. The MLS IWCs are derived from cloud-induced radiances (CIR) using modeled CIR-IWC relations based on the MLS 240 GHz measurements. Single IWC measurements from MLS at 147 and 215 hPa have a vertical resolution of ~3.5 km and a horizontal along- and cross-track resolutions of ~160 and ~2 km, respectively. The data presented in this article uses MLS version 1.5 (except that in Figure 7 which uses version 2.2) IWCs [*Livesey et al.*, 2006], which are very similar to the values used and discussed in *Li et al.* [2005]. In this version, the estimated precision for the IWC measurements is approximately 0.4, 1.0 and 4.0 (mg m^{-3}) at 100, 147, and 215 hPa, respectively, which account for combined instrument plus algorithm uncertainties associated with a single observation. MLS is thought to be sensitive to IWC between about 2 and 50 mg/m^3. It is important to note that the MLS IWC data has yet to be comprehensively validated. A detailed description and preliminary validation of the MLS IWC retrieval can be found in *Wu et al.* [2006; 2007].

Unless otherwise noted, the mean MLS values shown are computed from the total IWC amounts divided by the total number of measurements (including cloud free conditions) and binned onto a 4°× 8° latitude-longitude grid. While MLS retrievals are based on limb sounding, and thus provide some depiction of vertical structure, they cannot provide a robust estimate of total IWP since it does not sample the entire column. Figure 5 illustrates MLS' estimate of annual mean IWC at 215 hPa and the zonal average of their vertically-resolved values which essentially includes levels 100 hPa, 147 hPa, 215 hPa and 316 hPa. Very important to this study is the interpretation of what components of the frozen hydrometeors (e.g. snow, cloud ice) are represented in MLS IWC retrievals. Because in high IWC cases large hydrometeors produce strong attenuation, MLS cannot penetrate the entire cloud and its sensitivity to cloud ice begins to saturate. The saturated/degraded measurements significantly underestimate the IWC in these cases, which in turn makes MLS less sensitive to clouds with large amount of hydrometeors. A qualitative interpretation is that MLS tends to saturate for cloud systems that have significant amounts of larger frozen hydrometeors and thus tend to only reflect distributions – in magnitude – that are more characteristic of cloud ice alone.

ii) CloudSat

The Cloud Profiling Radar (CPR) on the CloudSat satellite is a 94 GHz, nadir-viewing radar measuring backscattered power from the Earth's surface and particles in the atmospheric column as a function of distance [*Stephens et al.*, 2002]. Measurements of radar backscatter are converted to calibrated geophysical data quantities (radar reflectivity factor), which are then used in retrievals of cloud and precipitation properties such as ice water content (IWC). During each 160 ms measurement interval, the CPR data are collected into a single vertical profile of backscattered power sampled over 125 range bins measuring 240 m each, creating a total data

window of 30 km. The distance from the satellite to the data window changes as a function of orbital location in order to guarantee that the window includes the Earth's surface, because surface reflectivity is a useful measurement in its own right and also serves as a constraint in some retrieval algorithms. Because the CPR does not scan, measurements consist of vertical profiles along the satellite ground track (over 37,000 per orbit), providing a vertical cross section of clouds and precipitation in the atmosphere. The CPR footprint is oblong, due to the along-track motion during the 160 ms measurement interval, with 6-dB dimensions of approximately 1.3 km across-track and 1.7 km along-track (with a slight dependence on latitude). The minimum detectable reflectivity is approximately -30 dBZ (varies slightly with location, season, and background). CloudSat orbits as part of the A-Train constellation of satellites, following approximately one minute behind Aqua, 15 seconds ahead of CALIPSO, and about 14 minutes ahead of Aura/MLS, although the forward limb sounding retrieval of MLS reduces the separation of samples to about 7 minutes. CloudSat has been operational since June 2006.

The current CloudSat retrieval for ice water content (IWC) (version 5.1, contained in release 4 [R04] of the CloudSat 2B-CWC-RO data product) uses an optimal estimation approach to retrieve parameters of the ice cloud particle size distribution based on measurements of radar reflectivity [*Austin et al.*, 2008]. A priori data constructed from a database of cloud microphysical measurements constrain the solution where the measurements cannot; the a priori data values are selected as a function of temperature, which is available to the retrieval based on ECMWF model data. The retrieval assumes a lognormal size distribution of cloud particles, retrieving all three distribution parameters for each radar resolution bin and calculating IWC and other quantities from the retrieved parameters. A similar retrieval is performed for liquid water content (LWC); the composite profile contained in the 2B-CWC-RO product is obtained by

using the LWC retrieval for bins warmer than 0°C, the IWC retrieval for bins colder than -20°C, and a linear combination of the two in the intermediate temperature range. The minimum detectable IWC is estimated to be approximately 5 mg m^{-3}, depending on the distribution parameters. A number of validation studies are examining the accuracy and performance of the CloudSat IWC retrieval compared to other algorithms and other platforms (comparisons to MLS, CRM studies, etc.). The annual mean IWP estimate from CloudSat is shown in Figure 4. Evident is that it is biased high relative to the other products, particularly in the tropical regions. Figure 5 illustrates CloudSat's estimate of annual mean IWC at 215 hPa and the zonal average of their vertically-resolved values which in this case include retrievals through the whole column. While the IWC retrieval algorithm does not consider larger species such as snow and graupel explicitly, the radar will certainly see these larger particles due to the powerful dependence of radar reflectivity on particle size (D^6 for Rayleigh particles, but less as particles move to the Mie scattering regime). Efforts are underway to determine the accuracy of the retrieved IWC values in the presence of these larger particles. Separate retrievals designed specifically for snow are also in preparation as experimental products.

iii) CALIPSO

The A-train also includes the Cloud – Aerosol LIDAR Infrared Pathfinder Satellite Observations (CALIPSO) instrument that is also expected to provide estimates of IWC based on lidar backscatter [*Winker et al.*, 2004; *Vaughan et al.*, 2004.]. In this case, the horizontal and vertical resolutions will be about 60 km and 1 km, respectively, and the sensitivity range is expected to be about 0.03 and 100 mg/m^3. At the time of this writing the CALIPSO IWC product is yet to be released.

c) Satellite Summary

One important distinction between the radar/limb-sounding and the nadir-viewing passive products discussed above is that the sampling of the former is only based on a single sub-orbital track profile, rather than a swath or multi-satellite product. Thus while the former gain in terms of vertically-resolved information, and in some cases higher horizontal resolution, their combined spatial-temporal sampling is considerably less.

The brief descriptions of the satellite data discussed above are only meant to highlight in a very brief manner the different techniques and their associated gross strengths and weaknesses. More detailed discussion of the techniques and shortcomings, along with pertinent validation procedures and results are given in the references cited above, see also Wu et al. [2007; 2008]. Overall, there are three messages to be conveyed from the above discussion. The first is that, until recently, the availability of global cloud ice estimates was limited to IWP based on passive infrared or microwave techniques (e.g., NOAA, CERES, MODIS, ISCCP). These products' known limitations and uncertainties, including their limited intercomparison and validation, have hampered their use in constraining modeled cloud ice values. However, it is noteworthy that the few observed satellite estimates of IWP that have been available for a number of years tend to exhibit agreement as good, and probably better, than the GCMs utilized in the most recent IPCC assessment (Figure 3). The second message is that more recent measurement strategies (e.g., limb-sounding and radar) are better equipped to probe and characterize internal cloud properties, such as vertical profiles of IWC, in addition to obtaining IWP. However, at first glance there appears to be considerable disagreement between these two new estimates of "cloud" IWC as well as disagreement between CloudSat IWP and those based on passive techniques. This raises the third message, considerable caution has to be applied when comparing these estimates due to

the various sensor and algorithm sensitivities. It is this latter issue that is a focal point of this article, namely in terms of understanding the nature of the ice water being measured and judiciously using these estimates for model diagnosis and validation.

3. Modeled Values

In a manner analogous to the previous section, the discussion in this section is meant to briefly describe the considerations typically in place within a GCM that account for the simulation of frozen hydrometeors in the atmosphere – both cloud ice and precipitating frozen particles. Relevant concepts and important distinctions include convective versus non-convective/stratiform clouds, diagnostic versus prognostic parameterizations, single versus multiple hydrometeor species, and single versus multi-moment characterizations. These issues are highlighted below and then the features of the ice-cloud parameterizations for the GCMs examined in this study are briefly described.

a) Overview

In GCMs, the atmospheric processes associated with convective clouds and non-convective clouds are artificially separated into cumulus convection and stratiform cloud schemes. For processes such as cumulus convection and cloud microphysics that occur at scales smaller than the GCM grid resolution (typically 50-200km), specific cloud variables are determined as a function of variables that are defined at the grid scale, leading to a so-called "parameterization". Most GCMs (excluding CRM-like frameworks described below) parameterize deep convection based on a convective mass fluxes approach. In this approach, temperature and humidity profiles are adjusted to account for heat sources and moisture sinks directly induced by the convective mass flux [*Arakawa and Schubert*, 1974; *Tiedtke*, 1989; *Gregory and Rowntree*, 1990; *Zhang*

and McFarlane, 1995]. Important to note is that due to the observed small spatial scales of cumulus convection, the influence they have on cloudiness and thus radiation has often been neglected with the main objective only being their direct impact on humidity and temperature via latent heating. Due to the large spatial scales of stratiform clouds, GCMs have generally accounted for "cloudiness", and its effect on radiation, via this part of the model's parameterization.

Studies have shown that non-convective stratiform clouds (e.g., widespread precipitating anvil clouds and cirrus outflow) can be produced by the detrainment of condensed water from cumulus convection. Such connections within a modeling context have been taken into account by coupling stratiform cloud and cumulus convection processes in GCMs [***Tiedke***, 1993]. More specifically, a link is made by including the effects of convection on cloud generation (i.e., convective detrainment as a source of large-scale cloud) and allowing dissipation of cloud particles directly during their formulation. This technique originates from attempts by Arakawa and Schubert [1974] to allow detrainment from convective cumulus towers to serve as a source for non-convective stratiform clouds. In general, non-convective stratiform clouds and their condensates are formed, maintained and dissipated by many processes such as small-scale turbulence, large-scale vertical motion, convection and cloud microphysical processes. Therefore, any coupling between convective and stratiform clouds requires reliable parameterizations of microphysical processes within the model's non-convective regions of stratiform clouds.

When modeling ice clouds, several processes must be considered in cloud schemes: the formation (e.g., nucleation, deposition) and possible sedimentation of clouds, the growth and interactions (e.g, deposition and riming, aggregation) and falling out of precipitation, the

evaporation/sublimation of both clouds and precipitation, and possibly advection of clouds and precipitation. Due to computational considerations as well as our incomplete knowledge of cloud-ice and related fields and their associated processes, most GCMs utilize fairly simple representations of ice processes. Figure 6 is a highly simplified schematic illustrating the most rudimentary features and considerations in these representations. It mainly distinguishes the highly simplified forms in typical GCMs (e.g., Figure 3) used for global weather forecasting as well as many forms of climate simulation (left) versus a somewhat common next level of sophistication (right). In the former, there is consideration of only a single species of condensate, "floating" cloud ice. Processes within the parameterization – relying on the large-scale fields – lead to the development and dissipation of the clouds. In some cases, the processes are treated rather empirically, and are implicit, in others they are more explicitly represented [*Jakob*, 2002]. Important in this class of parameterizations is that a fraction of condensate is typically assumed to have grown to a mass/particle size large enough to be considered precipitation, and is assumed to immediately fall out – albeit it can moisten lower layers through evaporation in this fall out process. In such cases, the GCM typically carries two primary cloud variables, horizontal cloud fraction and cloud condensate mass – where the latter is considered "floating" cloud ice. Such a formulation is also referred to as a single-moment cloud scheme, because the number concentration of the ice particles is prescribed and only the mass is predicted. More complex formulations, which are more common in regional and cloud-resolving models (CRMs), include double-moment parameterizations that also predict number concentrations, or even more computationally expensive spectral and bin microphysics that include multiple discrete ice particle sizes, number concentrations and explicit particle-particle interactions.

Another level of complexity beyond the simplified single-species representation in Figure 6 is allowing more ice condensate species (e.g., snow and graupel). A simplified representation of this is illustrated in the right side of Figure 6. In this case, cloud ice is distinguished from snow and graupel by a consideration of particle size and/or the amount of overall ice mass, and graupel is distinguished from snow via the ice growth process during its formation (i.e. deposition or riming). In these cases, there is typically a prescribed particle density for each species, or in more complex representations this can be predicted as well. In addition, schemes of this complexity typically take particle fall velocities into more careful consideration, with even the cloud ice subject to sedimentation.

A final notion to highlight is that cloud parameterization schemes can be diagnostic, prognostic or a combination of the two. In a diagnostic approach, cloud variables and the overall cloud state are determined as a function of other model variables (such as model resolved wind fields, temperature, water vapor and relative humidity etc.). For this type of approach, there is no cloud memory in successive model time steps and the relationships between the state of the cloud field and model state is fully determined. The simplest example of this kind, a grid-scale condensation scheme, produces clouds only when the GCM grid box mean relative humidity reaches a specified threshold [e.g., 100%, *Geleyn*, 1980]. In prognostic cloud schemes [e.g., *Sundqvist*, 1978], the time evolution of cloud variables (e.g., cloud-ice mass and cloud cover) is predicted based on contributions from: grid-scale advection of the cloud variable (e.g., through horizontal and vertical wind fields), source terms (e.g., cumulus convective cloud condensates detrainment) and sink terms (e.g., auto-conversion between cloud condensates and precipitation).

b) Models

For the GCMs utilized in this study, the following two subsections give brief descriptions of their parameterizations used to model ice clouds and related processes. The first subsection contains descriptions for what are simply referred to as GCMs, which typically rely on ice-cloud parameterizations of a rather simple form (e.g, left side of Figure 6). The second subsection contains descriptions of two GCMs where there is an attempt, through novel numerical/conceptual frameworks, to better resolve cumulus processes. In these two cases, the ice processes are based on the three-species approach discussed above (e.g, right side of Figure 6).

i) GCMs and Single Species: Cloud Ice

The ECMWF Integrated Forecast System (IFS; version 30R1) cloud scheme uses prognostic equations for cloud cover and total cloud condensate content (i.e., ice and liquid together). Condensed water species are considered pure ice at temperatures colder than -23 °C and liquid at temperatures warmer than freezing. Between -23 °C and 0 °C, the total cloud condensate is divided into ice and liquid mass by linearly scaling the fraction of the total condensate by temperature. Two kinds of ice crystals are modeled, "pure ice" (particles < 100 μm) and "snow" (particles > 100 μm). Snow falls out instantly upon formation but is subject to sublimation and melting in lower levels. Note that ice particles falling into a cloudy layer are a source for ice in that layer, whereas ice falling into clear sky is converted into snow. The scheme considers sources/sinks from convective and non-convective processes (e.g., turbulence near cloud edges and resolved-scale ascent/decent), with deep, shallow and mid-level convective processes represented. The condensates produced in convective updrafts can be detrained from the upper cloud layers into the environment. The formation of clouds by non-convective processes, on the

other hand, is determined by the balance between the specific humidity and its saturation value, resolved vertical ascent of moist air, and/or the diabatic cooling rate (e.g., longwave radiation). The scheme considers cloud destruction through evaporation associated with large-scale and cumulus-induced descent, diabatic heating (e.g., solar radiation) and turbulent mixing between cloudy air and environmental air near the cloud edge. Processes such as auto-conversion, collection and accretion are active in clouds, with evaporation of precipitation being the active process outside clouds. The falling/sedimentation rates of cloud condensate whether they are ice mass, mixed phase or pure water clouds depend on temperature and ice particle size. For this comparison, the IWC include the analyzed values from both the R30 and R31 versions of the IFS system, and include periods from 8/2005 to 7/2006.

The GEOS5 ice cloud scheme is prognostic for cloud condensate and cloud fraction. Two types of clouds are distinguished by their condensate source. Anvil clouds originate from detraining convection and large-scale clouds originate using a probability density function (PDF) based on condensation calculations. This scheme directly links convection to anvil cloud variables by allowing detrained mass and condensate fluxes from the convective scheme to be added to the existing condensate and fraction for the anvil cloud type. For the large-scale clouds, cloud condensation is estimated using a simple PDF of total water [*Smith*, 1990; *Rotstayn*, 1999] and used to update cloud fraction and condensate. The destruction processes include - evaporation of condensate and fraction, sedimentation of frozen condensate and accretion of condensate by falling precipitation. The evaporation of condensate and cloud fraction is meant to represent destruction of cloud along edges in contact with cloud-free air following Del Genio et al [1996]. Sedimentation speeds are calculated as in Lawrence and Crutzen [1998] except that their expression for mid-latitude clouds is applied to all ice clouds of the large-scale type, and their

expression for tropical clouds is applied to the anvil type. For this comparison, the IWCs are based on a simulation using specified sea surface temperatures (SSTs) for the period 1/1999-12/2002.

The NCAR Climate Atmosphere Model (CAM 3.0) cloud scheme uses prognostic equations for two predicted variables: liquid and ice phase condensate [***Rasch*** *and Kristjansson*, 1988; *Zhang and McFarlane*, 1995]. During each time step, however, these are combined into a total condensate and partitioned according to temperature (described below), but elsewhere function as independent quantities. The scheme considers condensate sources/sinks both from grid-scale (*e.g.* horizontal advective and vertical motions) and sub-grid scale (*e.g.* convective and turbulent) processes. The parameterization has two components: a macro-scale component that describes the exchange of water substance between the condensate and the vapor phase and the associated temperature change arising from that phase change [*Zhang et al.*, 2003], and a bulk microphysical component that controls the conversion from condensate to precipitate. In its bulk microphysics step, the total condensate is decomposed into liquid and ice phases and considered all ice if T < -40 ºC and all liquid if T > -10 ºC. At -40 ºC < T < -10 ºC, the phase is determined with a linear relation in between. Within the parameterization, four types of condensate may exist and are expressed as mixing ratios of liquid and ice phases for suspended condensate with minimal fall speed, and liquid and ice phases for falling condensate (i.e. precipitation). Only the suspended condensates are carried forward in time, with precipitation falling out instantaneously. Precipitation is formed by explicitly considering individual physical quantities like droplet or ice number concentration, shape of size distribution of precipitate, etc. The precipitate may be a mixture of rain and snow, and is treated in diagnostic form. In addition, the conversion from condensate to precipitate as well as the evaporation of condensate and precipitate are

parameterized. There is a direct link to the convective scheme even though the scheme itself does not include the ice phase (i.e., all detrained condensate is in liquid form). Convective detrainment can still contribute to the IWC of the large-scale clouds in the model at cold temperatures, with a portion of the detrained liquid partitioned into ice according to the temperature considerations given above. After convection processes and sedimentation have occurred, the liquid and ice mixing ratios are recalculated from the total cloud condensate. For the comparisons presented later in the paper, the IWC values have been generated by the CAM3 using specified sea surface temperatures (SSTs) for the period from 1979 to 1999.

ii) CRM-like GCMs with Multiple Frozen Species: Clouds, Snow and Graupel

This section describes two models that utilize the multi-species ice framework. These two models are of a different class of GCM, in that they try to more explicitly account for the representation of sub-grid scale processes. For this reason, they are referred to collectively in this study as Cloud-Resolving Model (CRM)-like GCMs. While this aspect deserves mention, the most relevant point of the discussion is that their ice microphysical schemes include representations of cloud ice, snow and graupel, which allow for an additional consideration in terms of the model-data comparisons. However, it is important to recognize that the CRM-like nature of these models is not a requisite to incorporating this three-species framework into a GCM.

In what is now commonly referred to as the multi-scale modeling framework (MMF; also known as "Super parameterization"), the conventional cloud parameterizations are replaced with a CRM in each host GCM grid column [*Grabowski*, 2001; *Khairoutdinov and Randall*, 2001; *Randall et al.*, 2003]. The MMF is designed such that the GCM provides large-scale forcing to a CRM within each GCM grid column. The CRM then provides subgrid fluxes, cumulus convection and

clouds etc. to the parent GCM. This allows for explicit simulation of cloud processes and their interactions with radiation and surface processes within the GCM, and a two-way interaction between the cumulus and large-scale. The NASA fvMMF was developed using a finite volume GCM (fvGCM) with 2^{o}x2.5^{o} resolution and a version of the two-dimensional (2D) Goddard Cumulus Ensemble (GCE) model [*Tao et al.*, 2003] embedded in each GCM grid box. The fvMMF employs a single-moment bulk microphysical scheme with two liquid (cloud and rain) and three frozen (cloud, snow and graupel) hydrometeor classes. This six-class (water vapor plus five hydrometers) bulk scheme includes comprehensive microphysical processes among the water vapor and hydrometeors. The density for solid hydrometeors are assumed to be 0.917, 0.1, 0.4 g cm^{-3} for cloud ice, snow and graupel, respectively (e.g., Figure 6). The sedimentation processes of precipitating condensates as well as cloud ice crystals are also considered. For this comparison, the IWC values are based on simulations with prescribed SSTs for the months 07/1998 and 01/1999.

Kuang et al. [2005] proposed a different kind of approach for improving the cumulus scale called Diabatic Acceleration and REscaling or Reduced Acceleration in the VErtical (DARE/RAVE) . DARE/RAVE is a computationally efficient method for simulating the interactions of large-scale atmospheric circulations with deep convection in a 3D cloud-resolving model by reducing the scale difference between the large-scale and convective circulations. Data used in this comparison are from a near-global (70^{o} N,S) prescribed SST simulation for the period 1998 using the Weather Research and Forecasting (WRF) model with the RAVE approach implemented (Kuang and Walker, manuscript in preparation). The horizontal grid spacing is ~80km, and the RAVE factor is 20. The microphysics scheme is a single-moment, 6-class microphysics scheme that includes the interaction between water vapor, cloud water, cloud ice,

rain, snow, and graupel [*Hong and Lim*, 2006]. In this case, the density for snow and graupel are assumed to be 0.1 and 0.5 g cm^{-3}, respectively, but not a quantity defined/used for cloud ice in this implementation.

4. Model-Data Comparisons

Before model-data comparisons can be made, a number of considerations have to be made in terms of sampling the model output in a manner that leads to the most meaningful comparison to the observations. In this section, we highlight some of the more notable issues, including sampling the model output to account for comparable populations and the influence of the diurnal cycle, and considerations of instrument/algorithm sensitivity associated with observed IWC thresholds and ranges. We then focus our discussion on the degree that all frozen hydrometeors are represented in the retrieved values as well as model representations. Aspects of the first two issues as they pertain to model-data comparisons between MLS and ECMWF analysis have been discussed in Li et al. [2007] and will only be touched on briefly here.

To illustrate the importance of proper sampling, Figure 7 shows the mean and the day minus night (i.e. 1:30pm – 1:30am local equatorial crossing time) difference in MLS IWC at 215 hPa. Evident is the impact of the strong diurnal cycle of deep convection over the tropical continents, accounting for fluctuations in IWC on the order of +/- 50% of the mean. Over the tropical oceans, convection typically peaks in the early morning, accounting for the opposite sign relative to the land. Figure 7 also shows a similar result based on CloudSat IWC values, with similar implications [cf., *Liu et al.*, 2008]. From this standpoint, it is obvious that a well-posed model-data comparison should take into account the diurnal sampling consistent with the satellite sensors – and thus it is necessary to sample the model output in accordance with the satellite

orbit. It should be noted here that of all the products mentioned in Section 2, a number of the cloud products based on ISCCP (albeit not IWC due to its reliance on visible channels) have the virtue of 3-hour sampling giving a much more robust depiction of the diurnal cycle. Future work might examine the virtues of combining the strengths of better time-resolved ISCCP cloud products with the more penetrating retrievals of IWC from CloudSat and MLS to construct a more comprehensive characterization of the diurnal cycle of IWC. Li et al. [2007] illustrated the impact of sampling the 4xdaily ECMWF analysis according to the MLS orbital sampling pattern. In that case, the satellite-sampled mean IWC at 215 hPa differed from the mean of the 4xdaily values in some tropical regions by up to 25%. Note that such a result will be strongly dependent on the model depictions of the diurnal cycle which have been shown to have significant shortcomings [*Yang and Slingo*, 2001; *Dai and Trenberth*, 2004].

A second, and significantly more complex issue that needs to be considered is the sensor and algorithm sensitivities in conjunction with the model representations. The upper panel of Figure 8 shows histograms for MLS IWC values at 147 hPa (green solid). Evident is the lower limit of MLS sensitivity at about 1.5 mg/m^3 and its upper limit of about 50 mg/m^3 that was mentioned in Section 2. Note that histograms for MLS data for a complete year (green solid) along with a single month (green dashed) of data are shown to illustrate that a month of (A-Train) sampling provides a representative sample when a large enough region is considered (in this case global, with the non-zero values effectively just coming from the tropics). Also shown is an analogous PDF from CloudSat (black solid) that shows the larger lower, and considerably larger upper, sensitivity limits relative to MLS. Note that both the MLS and CloudSat histograms are based on the inherent sensor footprint resolutions, with CloudSat's being a considerably smaller volume (see Section 2).

Values of IWC from two different recent versions of the ECMWF analysis are also shown (purple solid and dashed); the differences between the two versions will be discussed in more detail at the end of this section. The model(s) can have very small to near-zero values of IWC and in order to make a fair model-data comparison it may be necessary to set values that are less than the lower sensitivity limit to zero. Consideration may also be made in a similar way for the upper bound, meaning one might take model values larger than the upper sensitivity limit of the observations and reduce them to this (saturation) value. An example of accounting for such sensitivities in a model-data comparison is described in Li et al. [2007]. In that case, the ECMWF instantaneous (i.e. 4xdaily analyses) IWC values less than the MLS lower limit of sensitivity (e.g., 1.5 mg/m^3 at 215hPa) were set to zero before computing the time-mean values for comparison to MLS. The impact of the sensitivity sampling was less than 10%, but again, the impact in any given model-data combination will depend on both the model representation of the field (e.g., PDF) and the sensitivity limits of the given observation.

If consideration were made to perform the above procedure on the ECMWF data based on the histogram of the raw CloudSat retrievals, the differences would be greater than for the case of the MLS-applied sensitivity limits. This is because CloudSat's lower sensitivity limit is larger and thus a greater number of higher IWC values within the ECMWF would be set to zero leading to a greater impact on the mean ECMWF values. However, it is important to point out that for the MLS and ECMWF case described above, the model and satellite values have approximately the same spatial resolution (~100km) and thus they average over the similar sub-grid scale variability. On the other hand, CloudSat spatial resolution is considerably smaller – in fact one could say it is sampling the sub-grid scale of the MLS and ECMWF. To make a fair comparison, the CloudSat values need to be averaged to a comparable spatial resolution (black dashed).

Because this process averages "clear" (relative to CloudSat's lower sensitivity limit) and cloudy values, the lower sensitivity limit is no longer apparent. In fact in the low IWC regime, the ECMWF and 1°x1° CloudSat values show better agreement[1]. While a direct comparison may be more appropriate between these two curves (black dashed and purple lines), the two populations are still biased because nothing has yet been done to account for the lower sensitivity limit of CloudSat in this case.

Although this alone won't account for the intrinsic sampling mismatch just discussed, the most ideal manner of comparison is to construct from the model fields the radar reflectivity that would be observed by CloudSat and then perform the IWC retrieval on the constructed reflectivity (cf. ISCCP simulator**;** [*Klein and Jakob*, 1999; *Webb et al.*, 2001]). This approach has been used to assess CloudSat IWC retrievals from CRM output with multiple ice species [*Woods et al.*, 2008a] using a 94 GHz radar simulation package called QuickBeam [*Haynes et al.*, 2008]. To account for the possible spatial sampling mismatch, it would be best to average the observed reflectivity values over a grid-box comparable to the model resolution, then perform the cloud retrieval on them. Then from the PDF of this population, apply any lower and upper sensitivity limits of the sensor/algorithm to the model-derived values computed from the above approach.

While the above approach has its strengths, it is not conducive for assessing most climate and numerical weather prediction GCMs that only consider cloud ice and not other/larger frozen hydrometeors (e.g., snow and graupel). In such cases, the resultant reflectivity, and thus IWC retrieval, will be intrinsically unrealistic, or else can only be compared to observed cases where the larger hydrometeors are not expected or observed in the column. In a few cases, such as the

[1] Averaging CloudSat to 2°x2° makes only minor changes to the histogram relative to 1°x1° averaging.

NASA fvMMF and RAVE GCMs and regional cloud resolving models (CRMs), the additional constituents are modeled. This raises questions about what components of the frozen hydrometeors are represented by the observations, and then in turn, how they can be judiciously used to compare to the models. For example, in Section 2, it is mentioned that CloudSat is expected to be sensitive to these larger hydrometeors and thus represent more than just "floating" cloud ice water content. Meanwhile, the characteristics of MLS sampling (see Section 2) make it *appear* to be more representative of just the cloud ice. It is imperative to consider these issues to utilize the data for model comparison and validation.

Figure 9 shows zonal and annual mean values of IWC from three GCMs that only carry/simulate cloud ice, NCAR-CAM3, GEOS5, and ECMWF, in addition to the two CRM-like GCMs, RAVE and fvMMF. There are two main areas of disagreement amongst these models. First, there is discrepancy in the overall magnitude of about a factor of two to three. Second, their spatial distribution with respect to height is considerably different. Apart from their spatial distribution, it should be pointed out from Figure 8 that the PDF of the three cloud ice fields from GEOS5, ECMWF, and fvMMF have considerably different structures, particularly on the high end – although this part of the distribution is particularly sensitive to the grid resolution which are not identical in these models. These characteristics beg the question, do CloudSat and/or MLS data provide the means to discriminate which of these distributions is more realistic? Comparing to Figure 5, it is evident that the CloudSat zonal mean values are quite different, e.g., much larger in magnitude, than any of these model distributions. However, as mentioned above, CloudSat is expected to be sensitive to larger frozen hydrometeors that are not part of the representation in many model distributions, for example those shown in Figure 9. On the other hand, the magnitudes of the IWC in the MLS zonal average profile shown in Figure 5, which are thought

to be more representative of cloud ice for the reasons mentioned in Section 2, are much closer to the modeled values.

To shed additional light on these model-data comparisons, Figure 10 and Figure 11 show multi-component IWP distributions of the frozen hydrometeors simulated by two CRM-like GCMs, RAVE and fvMMF, respectively. For each model, the annual mean values of graupel, cloud ice, snow and total IWP are shown as horizontal maps. Also shown are the zonal mean values and the percent contribution of each constituent to the total. As there are yet no global observations that claim to readily distinguish these various components, the model distributions are being used here as somewhat of a guide, since their model microphysics were developed in consideration of field experiments/data, albeit temporally and spatially sparse. In general agreement between these two models are the following features: the total, graupel and snow IWP distributions have overall magnitudes that agree relatively well between the two models. There is a considerable difference in the magnitudes of the cloud IWP as was also evident in Figure 9. Beyond this there are considerable differences in the regional scale features of the distributions. Most important for this discussion, are the relative contributions of the various frozen hydrometeor components to the total IWP. In the RAVE GCM, each component represents about 30% of the total frozen mass in the tropics, while in the fvMMF, the graupel, snow and cloud are about 50%, 30% and 10%, respectively. Thus in the case of these two models, the overall message is that each of the three frozen components contributes a sizeable fraction to the overall total. If this is the case in nature, this must be considered in regards to applying the satellite observations, interpreting the model-data comparisons and in particular designing new observing systems. An interesting feature is that the magnitude and spatial distribution of the total IWP somewhat resembles the CloudSat IWP (and to some degree the MODIS and CERES) values that are shown in Figure 4,

with the reminder that CloudSat is sensitive and may be accounting for most of the larger frozen hydrometeors and larger IWC values.

Figure 12 shows the zonal and annual mean vertical profiles of IWC from the two CRM- GCMs. Except for the distributions of cloud ice, the distributions for the other frozen components from the two models agree relatively well, particularly given the complete lack of global observations that would adequately guide and constrain GCM development in this area. Notable is the relatively good agreement in the total IWC values in this figure, namely in terms of general morphology and magnitude, with those of CloudSat shown in Figure 5. Moreover, Figure 8 shows that there tends to be slightly better agreement between the CloudSat (1^{o}x1^{o}) PDF (black dashed) and the fvMMF total IWC (solid thick blue) than with that of any other constituent. However, one item worth pointing out is the differences in vertical distribution, particularly with respect to the tropics. For CloudSat, the greatest concentration of IWC is between 250 and 400 hPa, while for the models the peak values are found around 500-600 hPa. Presuming such distributions relate in some way to the latent and radiative heating profiles, this disagreement is somewhat troubling and might indicate shortcomings in the underlying microphysical schemes in these models as they relate to convection and the large-scale circulation. Consideration should also be given to the possibility that the height of the peak CloudSat values might also be artificially influenced by the algorithm's method of (linearly) combining the liquid and ice water retrieval solutions via temperature.

The results described above indicate that CloudSat IWC values may be a useful estimate of total IWP, at least for the purposes of representing a very preliminary and somewhat qualitative form of validation for models that carry a more comprehensive system of frozen hydrometeors. However, this still doesn't provide a constraint on the cloud ice component that is typically the

only component represented in many GCMs (i.e., Figure 6), and to the extent MLS might provide such a constraint, the latter is very limited in vertical extent. To help address this problem, it is possible to make judicious subsets of the CloudSat data based on additional flags and information in the retrieval products [*Stephens et al.*, 2008]. For example, Figure 13 shows CloudSat IWC values filtered in three different ways, taking only cases that are flagged as having no precipitation (NP) at the ground, classified as non-convective (NC) clouds, and the combination of both of these criteria (NP & NC). For example, the NP case includes all IWC = 0 (i.e. clear) and the only the IWC > 0 cases that are non-precipitating at the surface. The line plot on the lower left shows the frequency of occurrence of these three conditions. In the example just given, the frequency is calculated as the number of IWC > 0 cases that are non-precipitating divided by the *total* cases.

For interpretation of Figure 13, it is useful to start with the most stringently filtered case, i.e. NP & NC. In this case, the IWC is considerably lower than the total shown in Figure 5. In some regions, the reduction in IWC is well over 50% through the exclusion of the cases that exhibit precipitation at the surface and those denoted as convective. Both of these excluded cases would be expected to contain significant amounts of large frozen hydrometeors (e.g., snow, graupel). For the NC case, there is a significant increase in IWC in the mid-latitudes over the NP & NC case. Because the mid-latitude synoptic regime more readily allows for precipitation without convection, the IWC retained is considerably greater – in fact very near the original total in Figure 5. However, including the precipitating cases does not have a significant impact in the Tropics because most precipitation is associated with convection. This is why all three cases tend to be the same for the tropics, i.e. they retain only about 30% of total cloud ice observed by CloudSat (Figure 5). Interestingly, this fraction of retained ice – inferred here to be the

"floating" cloud ice – is within a factor of 2 or so of the same fraction of cloud to total ice as in the two CRM-like GCMs.

The main point of the discussion above is that with the additional constraints applied to CloudSat IWC, e.g., NP & NC, the values are more likely to reflect only ice content within clouds with significantly less contribution from graupel and snow [cf., *Stephens et al.*, 2008]. Additionally, these constrained values have a strong resemblance to the tropical values estimated by MLS. This can be seen by comparing the MLS IWC values shown in the inset panel of Figure 5 to the right of Figure 13 – which is the same as the left but plotted in a manner that can be more readily compared to the MLS values. The agreement between these two observational resources, along with an understanding of their sampling characteristics/constraints, indicates that these might serve as a preliminary guide for evaluating GCM-simulated (floating) cloud ice fields. One such comparison is derived by comparing the IWP estimate from CloudSat - with the NP & NC constraints applied - shown in Figure 14 to the GCM-simulated values of (cloud-only) IWP in Figure 3. This tentative comparison indicates that most of the models that contributed to the IPCC 4th assessment might underestimate cloud IWP.

A second comparison is given in Figure 15, which shows the IWC field at 215 hPa from MLS and from CloudSat with the NP & NC constraints applied, along with the GEOS5 and NCAR CAM3 GCMs, and the ECMWF R30 analysis. Within the context of this comparison, the two GCMs perform relatively well – considering the wide disparity displayed in the first MLS-GCM comparisons [*Li et al.*, 2005]. It is worth noting that while the ECMWF analysis R30 values are considerably less than the two satellite-derived values, efforts were undertaken to increase the cloud ice as well as upper-tropospheric water vapor through improved microphysics based on the arrival of MLS data and associated comparisons [*Li et al.*, 2007]. The improvement, relative to

the MLS estimates, is illustrated in Figure 16 and Figure 8. The changes in the cloud ice microphysics for this model (~ left side of Figure 6) involved allowing ice-phase supersaturation and a revision in the ice crystal sedimentation and snow auto-conversion rate [*Tompkins et al.*, 2007]. While the former condition would typically reduce the amount of IWC, the slowing of the rates in the latter revision accounted for the overall increase in IWC, and the better agreement with the satellite derived values.

6. Summary and Discussion

The accurate simulation of tropospheric ice clouds in GCMs continues to represent a significant challenge to the model development community. Shortcomings in the representation of these clouds impacts both the latent and radiative heating processes, and in turn the circulation and the energy and water cycles, leading to errors in weather and climate forecasts and to uncertainties in quantifying cloud feedbacks associated with global change (e.g., Figure 1 and Figure 3). Much of the challenge has been associated with a lack of high-quality, global observations of ice clouds and related quantities. While observations from passive nadir-viewing sensors have been available for some time (see Section 2), their cloud ice retrievals provide little vertical structure information (albeit 3 levels from ISCCP), have thus been generally limited to estimates of IWP, are severely hampered in multi-level cloud systems, and have undergone little systematic comparison and validation (e.g., Figure 2 and Figure 4). Despite these shortcomings, model development has progressed over the last decade in terms of more models including prognostic cloud schemes and introducing more sophisticated microphysics representations (e.g., Section 3 and Figure 6). With the arrival of the EOS-era of satellite observations, considerable new resources have become available to help address this problem. These include the moderate spectral and high spatial resolution of MODIS (see Section 2) and the stereoscopic capabilities of

MISR [*Diner et al.*, 1989]. Most relevant however to the challenges associated with cloud ice have been the products introduced by MLS and CloudSat, and soon CALIPSO (see Section 2). These latter products include vertically-resolved estimates of IWC (e.g., Figure 5) and have allowed for the first time global-scale comparisons of observed ice mass at a given level with GCM representations [*Li et al.*, 2005].

The arrival of these new cloud ice products heralds a new era for model diagnosis, development and validation with respect to cloud mass, structure and microphysical characterization. However, exploiting the observations comes with considerable challenges, since both the observing systems and the present model parameterizations and frameworks related to cloud ice have largely developed independently of each other. Thus, it is not a simple matter of comparing the model output with the retrieved quantities, as might be the case for more straightforward quantities like sea surface temperature, top of the atmosphere radiation, or total column water vapor. The algorithm teams are still in the process of characterizing and validating their observed estimates [*Wu et al.*, 2007; *Stephens et al.*, 2008] and GCMs exhibit considerable variation in their representations of ice clouds [e.g., Section 3, *Jakob*, 2002], meaning even comparisons amongst the observations themselves [e.g., Fig. 4, *Wu et al.*, 2008] or the models themselves is fraught with challenges. The background, results and discussion in this paper are meant to bring the model and satellite communities closer in order to make more rapid progress on this problem. Very fundamental yet basic information on the satellite side of the problem as well as the modeling side is presented so that greater common ground can be found for coordinating research and development in this area.

The most fundamental question addressed in this paper is can the MLS and/or CloudSat IWC be used to evaluate IWC values from GCMs? With this, comes discussion of what are the

considerations that must be made to make meaningful comparisons between the models and the observations. Inherent to this challenge is that the sensitivity and sampling characteristics of the instruments (e.g., Figure 7 and Figure 8) make their products only applicable to certain components and/or ranges of IWC. For example, MLS tends to represent IWC in the low to medium range of values (e.g., 2 to 50 mg m^{-3}), and because it samples only the upper most levels of the troposphere where precipitation and mixed-phase have less influence, might be most representative of the cloud ice field (see Section 2). On the other hand, CloudSat is much less sensitive to small IWC values and is sensitive to larger hydrometeors and IWC values.

Using our present understanding of the strengths and limitations of the IWC values from MLS and CloudSat, along with knowledge and findings regarding the model ice fields, the analysis works to constrain how the data can best be applied for model evaluation. A chief consideration is the degree the floating (i.e. cloud) and precipitating (e.g., snow, graupel) hydrometeor fields are represented. For example, typically GCMs represent and/or output the ice associated with clouds, with a few GCMs that explicitly represent precipitating hydrometeors as well (i.e. Figures 9-12). Based on the information at hand at this time and a number of qualitative inferences, the findings in this study lead to the suggestion that CloudSat IWC might provide a rough estimate of the total IWC field (i.e. including cloud, snow, graupel) that can be compared to GCMs that carry/simulate a more complete budget of the total ice field (Figures 4,5,10-12). In addition, MLS IWC, along with judiciously sampled CloudSat IWC, might provide a preliminary estimate of IWC associated with ice clouds in a GCM (Figures 13-16). Again, it has to be stressed that these products are still undergoing characterization and our community is just beginning to learn how to apply these retrievals to model-data comparisons. In any case, the limited capabilities of previous estimates (e.g., only IWP), coupled with their relatively poor

agreement (e.g., Figure 4), along with the critical need to provide *some* form of validation for what has largely been an unconstrained yet important quantity, dictates that even preliminary model-data comparisons along the lines discussed here be performed with these new resources.

There are a number of avenues that could and/or need to be explored in order to refine the types of preliminary comparisons presented in this study. On the observational side, additional validation studies, particularly those that may offer cross comparison and validation of MLS, CloudSat and CALIPSO, to help enhance confidence and characterization of the retrievals. The fact that these sensors fly in formation makes this a relatively productive and efficient undertaking. In addition, if more specific information could be relayed regarding a given product's applicability and/or sensitivity to quantities explicitly represented in models (e.g., cloud ice alone, snow, graupel), the easier it will be to extend and interpret these types of studies. Further, developing auxiliary products, such as the CloudSat cloud classification flags, and or learning to use other complementary A-Train sensors, may help immensely to characterize the context of the measurement and further refine the data-model comparison. For example, CloudSat provides particle size distribution (PSD) parameters as part of their retrievals. We have explored the use of these to reconstruct the size distribution and separate ice mass contributions from small and large particles to facilitate model-data comparisons [*Woods et al.*, 2008b]. Another very complimentary data set / methodology to explore in the present context is the hydrometer profile estimates from TRMM which are thought to represent precipitating ice particles [*Jiang and Zipser*, 2006]. As we continue to learn about the strengths of the current data and where hard limitations exist, follow-on mission design should be particularly cognizant of the model quantities and specific validation needs. Having additional microphysical

information (e.g., particle size) or dynamic information (e.g., vertical velocity) would be exceptionally helpful for further guiding and validating model development.

As with the observation side, a clear(er) articulation by the modelers of the mass and particle size ranges being represented in the cloud parameterizations is needed to make the model-data comparisons most meaningful. Similarly, for the models that tend to only represent and output their cloud ice values, it would be useful to output the ice mass that is presumed to have precipitated out on a level-by-level basis. This is a quantity that is not typically output but yet may provide through the use of CloudSat IWC an additional constraint on the model's ice physics. Beyond just getting the mean fields of ice mass correct, it will also be important to explore and validate in greater detail the distributions of ice mass values (e.g., Figure 8), paying close attention to equitable sampling methodologies. Finally, for those models that carry a more comprehensive range of frozen hydrometer mass (e.g., cloud, snow, graupel), it would be helpful if the modelers considered the incorporation or use of QuickBeam [*Haynes et al.*, 2008] and the CloudSat retrieval algorithm(s) to allow for a close correspondence between model and observed quantities. Overall the challenge is quite clear regarding our model simulations of cloud ice (e.g., Figure 1 and Figure 3) but given the new A-Train resources in hand, in conjunction with those from a number of others that bring complementary information (e.g., see those in Figure 4), we should expect to see a significant reduction in the shortcomings associated with our cloud ice simulations and in the uncertainties associated with (high) cloud climate change feedback by the time of the next IPCC assessment report. An encouraging sign is that ECMWF has already introduced changes that bring their IFS system into better alignment with the available observations, and the latter have also played a role in the recent development of the GEOS5

GCM which also exhibits quantitatively good model-data agreement (e.g., Figure 15 and Figure 16).

Acknowledgements

The research described in this paper was carried out at the Jet Propulsion Laboratory, California Institute of Technology, under a contract with the National Aeronautics and Space Administration (NASA). It was also supported by NASA through the CloudSat and CALIPSO programs. The authors would like to acknowledge support from Brent Maddux and Steve Ackerman for assistance with MODIS MYD06 analysis.

References

Ackerman, S. A., R. E. Holz, R. Frey, E. W. Eloranta, B. Maddux, and M. McGill (2008), Cloud Detection with MODIS: Part II Validation, *Journal of Atmospheric and Ocean Technology*, In Press.

Arakawa, A., and W. H. Schubert (1974), Interaction of a Cumulus Cloud Ensemble with Large-Scale Environment .1, *Journal of the Atmospheric Sciences*, *31*(3), 674-701.

Arkin, P. A., and P. E. Ardanuy (1989), Estimating Climatic-Scale Precipitation from Space - a Review, *J. Clim.*, *2*(11), 1229-1238.

Austin, R. T., A. J. Heymsfield, and G. L. Stephens (2008), Retrievals of ice cloud microphysical parameters using the CloudSat millimeter-wave radar and temperature, *J. Geoph. Res.*, *Submitted*.

Baum, B. A., P. Yang, A. J. Heymsfield, S. Platnick, M. D. King, Y.-X. Hu, and S. T. Bedka (2005), Bulk scattering properties for the remote sensing of ice clouds II: Narrowband Models., *Journal of Applied Meteorology*, *44*, 1896-1911.

Chen, T., W. B. Rossow, and Y. C. Zhang (2000), Radiative effects of cloud-type variations, *J. Clim.*, *13*(1), 264-286.

Chiriaco, M., H. Chepfer, P. Minnis, M. Haeffelin, S. Platnick, D. Baumgardner, P. Dubuisson, M. McGill, V. Noel, J. Pelon, D. Spangenberg, S. Sun-Mack, and G. Wind (2007), omparison of CALIPSO-like, LaRC, and MODIS retrievals of ice cloud properties over SIRTA in France and Florida during CRYSTAL-FACE, *Journal of Applied Meteorology and Climatology*, *46*, 249-272.

Dai, A. G., and K. E. Trenberth (2004), The diurnal cycle and its depiction in the Community Climate System Model, *J. Clim.*, *17*(5), 930-951.

Del Genio, A. D., M.-S. Yao, W. Kovari, and K. K.-W. Lo (1996), A prognostic cloud water parameterization for global climate models. , *J. Climate*, *9*, 270-304.

Del Genio, A. D., and W. Kovari (2002), Climatic properties of tropical precipitating convection under varying environmental conditions, *J. Clim.*, *15*(18), 2597-2615.

Diner, D. J., C. J. Bruegge, J. V. Martonchik, T. P. Ackerman, R. Davies, S. A. W. Gerstl, H. R. Gordon, P. J. Sellers, J. Clark, J. A. Daniels, E. D. Danielson, V. G. Duval, K. P. Klaasen, G. W. Lilienthal, D. I. Nakamoto, R. J. Pagano, and T. H. Reilly (1989), Misr - a Multiangle Imaging Spectroradiometer for Geophysical and Climatological Research from Eos, *Ieee Transactions on Geoscience and Remote Sensing*, *27*(2), 200-214.

Ferraro, R. R., F. Weng, N. Grody, L. Zhao, H. Meng, C. Kongoli, P. Pellegrino, S. Qiu, and C. Dean (2005), NOAA operational hydrological products derived from the AMSU, *IEEE Trans. Geo. Rem. Sensing*, *43*, 1036 – 1049.

Frey, R. A., S. A. Ackerman, Y. Liu, K. I. Strabala, H. Zhang, J. Key, and X. Wang (2008), Cloud Detection with MODIS, Part I: Recent Improvements in the MODIS Cloud Mask, *Journal of Atmospheric and Ocean Technology*, *In Press*.

Fu, Q., and K. N. Liou (1992), On The Correlated K-Distribution Method For Radiative-Transfer In Nonhomogeneous Atmospheres, *Journal Of The Atmospheric Sciences*, *49*(22), 2139-2156.

Geleyn, J.-F. (1980), :Some diagnostics of the cloud/radiation interaction in the ECMWF forecasting model, paper presented at ECMWF Workshop on 'Radiation and cloud-radiation interaction in numerical modelling, 135-162.

Grabowski, W. W. (2001), Coupling cloud processes with the large-scale dynamics using the Cloud-Resolving Convection Parameterization (CRCP), *Journal of the Atmospheric Sciences*, *58*(9), 978-997.

Gregory, D., and P. R. Rowntree (1990), A mass flux convection scheme with representation of cloud ensemble characteristics and stability-dependent closure, *Monthly Weather Review*, *118*, 1483-1506.

Gruber, A., and A. F. Krueger (1984), THE STATUS OF THE NOAA OUTGOING LONGWAVE RADIATION DATA SET, *Bull. Amer. Meteor. Soc.*, *65*(9), 958-962.

Han, Q. Y., W. B. Rossow, J. Chou, K. S. Kuo, and R. M. Welch (1999), The effects of aspect ratio and surface roughness on satellite retrievals of ice-cloud properties, *Journal of Quantitative Spectroscopy & Radiative Transfer*, *63*(2-6), 559-583.

Hartmann, D. L., and D. A. Short (1980), On The Use Of Earth Radiation Budget Statistics For Studies Of Clouds And Climate, *Journal Of The Atmospheric Sciences*, *37*(6), 1233-1250.

Hartmann, D. L., and D. Doelling (1991), On The Net Radiative Effectiveness Of Clouds, *J. Geoph. Res. - Atmos.*, *96*(D1), 869-891.

Hartmann, D. L., M. E. Ockertbell, and M. L. Michelsen (1992), The Effect Of Cloud Type On Earths Energy-Balance - Global Analysis, *J. Clim.*, *5*(11), 1281-1304.

Haynes, J. M., R. T. Marchand, Z. Luo, A. Bodas-Sakedo, and G. L. Stephens (2008), A multi-purpose radar simulation package: QuickBeam, *Bull. Amer. Meteor. Soc.*, *In Press*.

Hong, S.-Y., and J.-O. J. Lim (2006), The WRF Single-Moment 6-Class Microphysics Scheme (WSM6) *JOURNAL OF THE KOREAN METEOROLOGICAL SOCIETY*, *42*, 129-151

Huang, J., P. Minnis, B. Lin, Y. Yi, T.-F. Fan, S. Sun-Mack, and J. K. Ayers (2006), Determination of ice water path in ice-over-water cloud systems using combined MODIS

and AMSR-E measurements, *Geophys. Res. Lett.*, *33*, L21801, 21810.21029/22006GL027038.

IPCC (2007), Climate Change 2007: The Physical Science Basis. Contribution of Working Group I to the Fourth Assessment Report of the Intergovernmental Panel on Climate Change [Solomon, S., D. Qin, M. Manning, Z. Chen, M. Marquis, K.B. Averyt, M.Tignor and H.L. Miller (eds.)]. Cambridge University Press, Cambridge, United Kingdom and New York, NY, USA.

Jakob, C. (2002), Ice clouds in Numerical Weather Prediction models - progress, problems and prospects, in *Cirrus*, edited by D. K. Lynch, pp. 327-345, Oxford University Pres.

Jiang, H., and E. J. Zipser (2006), Retrieval of hydrometeor profiles in tropical cyclones and convection from combined radar and radiometer observations, *Journal of Applied Meteorology and Climatology*, *45*, 1096-1115.

Jin, Y., W. B. Rossow, and D. P. Wylie (1996), Comparison of the climatologies of high-level clouds from HIRS and ISCCP, *J. Clim.*, *9*(11), 2850-2879.

Jin, Y., and W. B. Rossow (1997), Detection of cirrus overlapping low-level clouds, *J. Geoph. Res. - Atmos.*, *102*(D2), 1727-1737.

Khairoutdinov, M. F., and D. A. Randall (2001), A cloud resolving model as a cloud parameterization in the NCAR Community Climate System Model: Preliminary results, *Geophys. Res. Lett.*, *28*(18), 3617-3620.

Kiehl, J. T. (1994), On The Observed Near Cancellation Between Longwave And Shortwave Cloud Forcing In Tropical Regions, *J. Clim.*, *7*(4), 559-565.

King, M. D., W. P. Menze, Y. J. Kaufman, D. Tanre, B.-C. Gao, S. Platnick, S. A. Ackerman, L. A. Remer, R. Pincus, and P. A. Hubanks (2003), Cloud and aerosol properties, precipitable

water, and profiles of temperature and humidity, *IEEE Trans. Geosci. Remote Sens.*, *41*(442-458).

King, M. D., S. Platnick, P. Yang, G. T. Arnold, M. A. Gray, J. C. Riedi, S. A. Ackerman, and K. N. Liou (2004), Remote sensing of liquid water and ice cloud optical thickness and effective radius in the Arctic: Application of airborne multispectral MAS data, *Journal of Atmospheric and Ocean Technology*, *21*, 857-875.

Klein, S. A., and C. Jakob (1999), Validation and sensitivities of frontal clouds simulated by the ECMWF model, *Monthly Weather Review*, *127*(10), 2514-2531.

Krueger, S. K., Q. A. Fu, K. N. Liou, and H. N. S. Chin (1995), Improvements Of An Ice-Phase Microphysics Parameterization For Use In Numerical Simulations Of Tropical Convection, *Journal Of Applied Meteorology*, *34*(1), 281-287.

Kuang, Z., P. N. Blossey, and C. S. Bretherton (2005), A DARE approach for 3D cloud resolving simulations of large scale atmospheric circulation, *Geophys. Res. Lett.*, *32*, L02809, 02810.01029/02004GL021024.

Kyle, H. L., J. R. Hickey, P. E. Ardanuy, H. Jacobowitz, A. Arking, G. G. Campbell, F. B. House, R. Maschhoff, G. L. Smith, L. L. Stowe, and T. Vonderhaar (1993), THE NIMBUS EARTH RADIATION BUDGET (ERB) EXPERIMENT - 1975 TO 1992, *Bull. Amer. Meteor. Soc.*, *74*(5), 815-830.

Lawrence, M. G., and P. J. Crutzen (1998), The impact of cloud particle gravitational settling on soluble trace gas distributions, *Tellus (B Chem. Phys. Meteorol.)*, *50B*, 263-289.

Li, J. L., D. E. Waliser, J. H. Jiang, D. L. Wu, W. Read, J. W. Waters, A. M. Tompkins, L. J. Donner, J. D. Chern, W. K. Tao, R. Atlas, Y. Gu, K. N. Liou, A. Del Genio, M. Khairoutdinov, and A. Gettelman (2005), Comparisons of EOS MLS cloud ice

measurements with ECMWF analyses and GCM simulations: Initial results, *Geophys. Res. Lett.*, *32*(18).

Li, J. L., J. H. Jiang, D. E. Waliser, and A. M. Tompkins (2007), Assessing consistency between EOS MLS and ECMWF analyzed and forecast estimates of cloud ice, *Geophys. Res. Lett.*, *34*(8).

Liao, X. H., W. B. Rossow, and D. Rind (1995a), Comparison between Sage-Ii and Isccp High-Level Clouds .2. Locating Cloud Tops, *J. Geoph. Res. - Atmos.*, *100*(D1), 1137-1147.

Liao, X. H., W. B. Rossow, and D. Rind (1995b), Comparison between Sage-Ii and Isccp High-Level Clouds .1. Global and Zonal Mean Cloud Amounts, *J. Geoph. Res. - Atmos.*, *100*(D1), 1121-1135.

Lin, B., and W. B. Rossow (1996), Seasonal variation of liquid and ice water path in nonprecipitating clouds over oceans, *J. Clim.*, *9*(11), 2890-2902.

Liou, K. N. (1975), Can Changes In Cloud Thickness Be Monitored From Satellite-Brightness Measurements, *Journal Of Applied Meteorology*, *14*(4), 644-645.

Liou, K. N. (1976), Absorption, Reflection And Transmission Of Solar-Radiation In Cloudy Atmospheres, *Journal Of The Atmospheric Sciences*, *33*(5), 798-805.

Liou, K. N., and S. C. Ou (1989), The Role Of Cloud Microphysical Processes In Climate - An Assessment From A One-Dimensional Perspective, *J. Geoph. Res. - Atmos.*, *94*(D6), 8599-8607.

Liu, C., J. E, Zipser, and S.W.Nesbitt (2007), Global distribution of tropical deep convection: Differences using infrared and radar as the primary data source. , *J. Climate*, *20*(,), 489-503, DOI:410.1175/JCLI4023.1171.

Liu, C., E. J. Zipser, G. G. Mace, and S. Benson (2008), Implications of the differences between daytime and nighttime CloudSat observations over the tropics, *J. Geoph. Res.*, *Submitted*.

Livesey, N. J., W. V. Snyder, W. G. Read, and P.A. Wagner (2006), Retrieval algorithms for the EOS Microwave Limb Sounder (MLS) instrument, *IEEE Trans. Geosci. Remote Sensing*, *44*(5), 1144-1155.

Luo, Z. Z., and W. B. Rossow (2004), Characterizing tropical cirrus life cycle, evolution, and interaction with upper-tropospheric water vapor using lagrangian trajectory analysis of satellite observations, *J. Clim.*, *17*(23), 4541-4563.

Mace, G. G., Y. Zhang, S. Platnick, M. D. King, P. Minnis, and P. Yang (2005), Evaluation of cirrus cloud properties from MODIS radiances using cloud properties derived from ground-based data collected at the ARM SGP site, *Journal of Applied Meteorology*, *44*, 221-240.

McFarquhar, G. M., and A. J. Heymsfield (1996), Microphysical characteristics of three anvils sampled during the central equatorial Pacific experiment, *Journal Of The Atmospheric Sciences*, *53*(17), 2401-2423.

McFarquhar, G. M., A. J. Heymsfield, J. Spinhirne, and B. Hart (2000), Thin and subvisual tropopause tropical cirrus: Observations and radiative impacts, *Journal Of The Atmospheric Sciences*, *57*(12), 1841-1853.

Miller, R. L. (1997), Tropical thermostats and low cloud cover, *J. Clim.*, *10*(3), 409-440.

Minnis, P., K. N. Liou, and Y. Takano (1993), Inference of cirrus cloud properties using satellite-observed visible and infrared radiances, 1: Parameterization of radiance fields,, *Journal o the Atmospheric Sciences*, *50*(9), 1279-1304.

Minnis, P., D. P. Kratz, J. J. A. Coakley, M. D. King, D. Garber, P. Heck, S. Mayor, D. F. Young, and R. Arduini (1995), Cloud Optical Property Retrieval (Subsystem 4.3). "Clouds

and the Earth's Radiant Energy System (CERES) Algorithm Theoretical Basis Document, Volume III: Cloud Analyses and Radiance Inversions (Subsystem 4)", NASA RP 1376 Vol. 3, edited by CERES Science Team, pp. 135-176.

Minnis, P., D. P. Garber, D. F. Young, R. F. Arduini, and Y. Takano (1998), Parameterization of reflectance and effective emittance for satellite remote sensing of cloud properties, *Journal of the Atmospheric Sciences*, *55*, 3313-3339.

Minnis, P., and e. al. (2007), Cloud property retrieval techniques for CERES using TRMM VIRRS and Terra and Aqua MODIS data, *IEEE Trans. Geo. Rem. Sensing*, *Submitted*.

Minnis, P., J. Huang, B. Lin, Y. Yi, R. F. Arduini, T.-F. Fan, J. K. Ayers, and G. G. Mace (2007), Ice cloud properties in ice-over-water cloud systems using TRMM VIRS and TMI data, *J. Geoph. Res.*, *112*, D06206, doi:06210.01029/02006JD007626.

Platnick, S., M. D. King, S. A. Ackerman, W. P. Menzel, B. A. Baum, J. C. Riédi, and R. A. Frey (2003), The MODIS Cloud Products: Algorithms and Examples from Terra, *IEEE Transactions on Geoscience and Remote Sensing*, *41*, 459-473.

Ramanathan, V., R. D. Cess, E. F. Harrison, P. Minnis, B. R. Barkstrom, E. Ahmad, and D. Hartmann (1989), Cloud-Radiative Forcing And Climate - Results From The Earth Radiation Budget Experiment, *Science*, *243*(4887), 57-63.

Ramanathan, V., and W. Collins (1991), Thermodynamic Regulation Of Ocean Warming By Cirrus Clouds Deduced From Observations Of The 1987 El-Nino, *Nature*, *351*(6321), 27-32.

Randall, D., M. Khairoutdinov, A. Arakawa, and W. Grabowski (2003), Breaking the cloud parameterization deadlock, *Bull. Amer. Meteor. Soc.*, *84*(11), 1547-+.

Randall, D. A., and S. Tjemkes (1991), Clouds, The Earths Radiation Budget, And The Hydrologic-Cycle, *Global Planet. Change*, *90*(1-3), 3-9.

Rasch, P. J., and J. E. Kristjansson (1988), A comparison of the CCM3 model climate using diagnosed and predicted condensate parameterizations. , *J. Clim.*, *11*, 1587–1614.

Rossow, W. B., and R. A. Schiffer (1991), Isccp Cloud Data Products, *Bull. Amer. Meteor. Soc.*, *72*(1), 2-20.

Rossow, W. B., and L. C. Garder (1993), Validation of Isccp Cloud Detections, *J. Clim.*, *6*(12), 2370-2393.

Rossow, W. B., and R. A. Schiffer (1999), Advances in understanding clouds from ISCCP, *Bull. Amer. Meteor. Soc.*, *80*(11), 2261-2287.

Rotstayn, L. D. (1999), Indirect forcing by anthropogenic aerosols: A global climate model calculation of the effective-radius and cloud-lifetime effects, *J. Geoph. Res.*, *104*, 9369-9380.

Smith, G. L., B. R. Barkstrom, E. F. Harrison, R. B. Lee, and B. A. Wielicki (1993), RADIATION BUDGET MEASUREMENTS FOR THE EIGHTIES AND NINETIES, in *Global Change and Space Observations*, edited, pp. 81-84.

Smith, R. N. B. (1990), A scheme for predicting layer clouds and their water content in a general circulation model, *Quarterly Journal of the Royal Meteorological Society*, *116:* , 435-460.

Soden, B. J. (2004), The impact of tropical convection and cirrus on upper tropospheric humidity: A Lagrangian analysis of satellite measurements, *Geophys. Res. Lett.*, *31*(20).

Soden, B. J., A. J. Broccoli, and R. S. Hemler (2004), On the use of cloud forcing to estimate cloud feedback, *J. Clim.*, *17*(19), 3661-3665.

Stephens, G. L., G. G. Campbell, and T. H. Vonderhaar (1981), Earth Radiation Budgets, *Journal of Geophysical Research-Oceans and Atmospheres*, *86*(NC10), 9739-9760.

Stephens, G. L., D. L. Jackson, and J. J. Bates (1994), A Comparison of Ssm/I and Tovs Column Water-Vapor Data over the Global Oceans, *Meteorology and Atmospheric Physics*, *54*(1-4), 183-201.

Stephens, G. L., D. G. Vane, R. J. Boain, G. G. Mace, K. Sassen, Z. E. Wang, A. J. Illingworth, E. J. O'Connor, W. B. Rossow, S. L. Durden, S. D. Miller, R. T. Austin, A. Benedetti, and C. Mitrescu (2002), The cloudsat mission and the a-train - A new dimension of space-based observations of clouds and precipitation, *Bull. Amer. Meteor. Soc.*, *83*(12), 1771-1790.

Stephens, G. L., D. G. Vane, S. Tanelli, E. Im, S. Durden, M. Rokey, D. Reinke, P. Partain, G. G. Mace, R. Austin, T. L'Ecuyer, J. Haynes, M. Lebsock, K. Suzuki, D. Waliser, D. Wu, J. Kay, A. Gettleman, and Z. Wang (2008), The CloudSat Mission: Performance and early science after the first year of operation, *J. Geoph. Res.*, *Submitted*.

Stubenrauch, C. J., W. B. Rossow, N. A. Scott, and A. Chedin (1999), Clouds as seen by satellite sounders (3I) and imagers (ISCCP). Part III: Spatial heterogeneity and radiative effects, *J. Clim.*, *12*(12), 3419-3442.

Sundqvist, H. (1978), A parameterization scheme for non-convective condensation including prediction of cloud water content, *Quarterly Journal of the Royal Meteorological Society*, *104*, 677-690.

Tao, W. K., J. Simpson, D. Baker, S. Braun, M. D. Chou, B. Ferrier, D. Johnson, A. Khain, S. Lang, B. Lynn, C. L. Shie, D. Starr, C. H. Sui, Y. Wang, and P. Wetzel (2003), Microphysics, radiation and surface processes in the Goddard Cumulus Ensemble (GCE) model, *Meteorology And Atmospheric Physics*, *82*(1-4), 97-137.

Tiedke, M. (1993), Representation of clouds in large-scale models, *Mon. Wea. Rev*, *121*, 3040-3061.

Tiedtke, M. (1989), A Comprehensive Mass Flux Scheme for CumulusParametrization in Large-Scale Models, *Monthly Weather Review*, *117*(1779-1800).

Tompkins, A. M., K. Gierens, and G. R¨adel (2007), Ice supersaturation in the ECMWF integrated forecasting system, *Quarterly Journal of the Royal Meteorological Society*, *133, 53–56, 2007.*

Vaughan, M., S. Young, D. Winker, K. Powell, A. Omar, Z. Liu, Y. Hu, and C. A. Hostetler (2004.), Fully automated analysis of space-based lidar data: an overview of the CALIPSO retrieval algorithms and data products. , *Proceedings of the Society of Photo-Optical Instrumentation Engineers*, *5575*, 16-30.

Webb, M., C. Senior, S. Bony, and J. J. Morcrette (2001), Combining ERBE and ISCCP data to assess clouds in the Hadley Centre, ECMWF and LMD atmospheric climate models, *Clim. Dyn.*, *17*(12), 905-922.

Wielicki, B. A., B. R. Barkstrom, B. A. Baum, T. P. Charlock, R. N. Green, D. P. Kratz, R. B. Lee, P. Minnis, G. L. Smith, T. M. Wong, D. F. Young, R. D. Cess, J. A. Coakley, D. A. H. Crommelynck, L. Donner, R. Kandel, M. D. King, A. J. Miller, V. Ramanathan, D. A. Randall, L. L. Stowe, and R. M. Welch (1998), Clouds and the Earth's Radiant Energy System (CERES): Algorithm overview, *Ieee Transactions On Geoscience And Remote Sensing*, *36*(4), 1127-1141.

Winker, D. M., W. H. Hunt, and C. A. Hostetler (2004), Status and Performance of the CALIPSO Lidar, *Proceedings of the Society of Photo-Optical Instrumentation Engineers*, *5575*, 8-15.

Woods, C., D. Waliser, J.-L. Li, R. Austin, G. Stephens, and D. Vane (2008a), Evaluating CloudSat Ice Water Retrievals Using a Cloud Resolving Model: Sensitivities to Frozen Particle Properties, *J. Geoph. Res.*, *Submitted*.

Woods, C. P., J.-L. Li, D. E. Waliser, and A. Tompkins (2008b), Partitioning CloudSat Ice Water Content for Comparison with Upper-Tropospheric Cloud Ice in Global Atmospheric Models, *Geophys. Res. Lett.*, *In Preparation*.

Wu, D. L., W. G. Read, A. E. Dessler, S. C. Sherwood, and J. H. Jiang (2005), UARS/MLS cloud ice measurements: Implications for H2O transport near the tropopause, *Journal Of The Atmospheric Sciences*, *62*(2), 518-530.

Wu, D. L., J. H. Jiang, and C. P. Davis (2006), EOS MLS cloud ice measurements and cloudy-sky radiative transfer model, *EEE GRS Aura Special Issue*, *44*(5), 1156-1165.

Wu, D. L., J. H. Jiang, R. T. Austin, M. Deng, S. L. Durden, A. J. Heymsfield, B. H. Kahn, J.-L. Li, G. G. Mace, G. M. McFarquhar, C. J. Nankervis, H. C. Pumphrey, W. G. Read, G. L. Stephens, S. Tanelli, D. G. Vane, D. E. Waliser, and J. W. Waters (2007), Aura MLS Cloud Ice Measurements and Comparisons with CloudSat and Other Correlative Data, *J. Geoph. Res.*, Submitted.

Wu, D. L., R. T. Austin, M. D. L. Durden, A. J. Heymsfield, J.-L. Li, G. M. McFarquhar, J. V. Pittman, G. L. Stephens, S. Tanelli, D. G. Vane, and D. E. Waliser (2008), Comparisons of Global Cloud Ice from MLS, CloudSat, and Correlative Data Sets, *J. Geoph. Res.*, *Submitted*.

Wylie, D. P., and P.-H. Wang (1997), Comparison of cloud frequency data from the High-resolution Infrared Radiometer Sounder and the Stratospheric Aerosol and Gas Experiment II. , *J. Geoph. Res.*, *102*, .29,893-829,900.

Wylie, D. P., and P. H. Wang (1999), Comparison of SAGE-II and HIRS co-located cloud height measurements, *Geophys. Res. Lett.*, *26*(22), 3373-3375.

Xie, P. P., and P. A. Arkin (1997), Global precipitation: A 17-year monthly analysis based on gauge observations, satellite estimates, and numerical model outputs, *Bull. Amer. Meteor. Soc.*, *78*(11), 2539-2558.

Yang, G. Y., and J. Slingo (2001), The diurnal cycle in the Tropics, *Monthly Weather Review*, *129*(4), 784-801.

Zhang, G. J., and N. A. McFarlane (1995), Sensitivity of climate simulations to the parameterization of cumulus convection in the Canadian Climate Centre General-Circulation Model, *Atmos.-Ocean*, *33*, 407-446.

Zhang, M. H., W. Y. Lin, C. S. Bretherton, J. J. Hack, and P. J. Rasch (2003), A modified formulation of fractional stratiform condensation rate in the NCAR Community Atmospheric Model (CAM2), *J. Geoph. Res. - Atmos.*, *108*(D1).

Zhao, L., and F. Weng (2002), Retrieval of Ice Cloud Parameters Using the Advanced Microwave Sounding Unit, *Journal of Applied Meteorology*, *41*, 384-395.

FIGURE CAPTIONS

Figure 1. Globally-averaged, annual mean values of precipitation, precipitable water, total cloud fraction and cloud ice water path from the 1970-1994 period of the 20th century GCM simulations contributed to the IPCC 4th Assessment Report (20c3m scenario). Zero values indicate that the given model did not provide this variable to the IPCC database.

Figure 2. Schematic diagram illustrating measurement methods for estimating cloud ice water content/path, including in-situ measurements as well as passive, radar and limb-sounding satellite techniques.

Figure 3. Annual mean values of cloud ice water path (IWP; gm m^{-2}) from the 1970-1994 period of the 20th century GCM simulations contributed to the IPCC 4th Assessment Report (20c3m scenario); Note that the color scale is not linear.

Figure 4. Annual mean values of cloud ice water path (IWP; gm m^{-2}) from ISCCP (upper left; 2005), NOAA/NESDIS (middle left; 2000-2006), CERES/MODIS (lower left; 2001-2005), MODIS MYD06 (upper right; 7/2002-6/2007), and CloudSat (middle right; 8/2006-7/2007). See text for details. Note that the color scale differs from that in Figure 3.

Figure 5. Annual mean values of cloud ice water content (IWC) at 215 hPa (left) and zonal average (right) from MLS (upper; 8/2004-7/2007) and CloudSat (lower; 8/2006-7/2007). For upper right panel, MLS retrievals only extend down to 316 hPa (dotted line); inset shows same MLS data as larger panel but with different color scale. Note that MLS data below 215 hPa for this version (1.5) is not part of the official release and was processed offline as an experimental product.

Figure 6. Schematic diagram illustrating basic features of model parameterizations of cloud-related ice for a conventional GCM using a single species microphysics scheme (left) and a 3-species microphysics scheme (right). The vertical axes are associated with ice growth processes and the horizontal axes are associated with ice mass and/or particle diameter and also particle fall velocity. On the left figure, ice growth processes are not distinguished and are all embedded within the simplified parameterization. On the right figure, deposition is the primary process associated with cloud and snow, while riming is the primary processes responsible for graupel formation. On the left figure, cloud ice is assumed to be floating, i.e. zero fall velocity, and the ice deemed to be precipitating is removed immediately, i.e. infinite fall velocity. Shading is an indication of the density of particles.

Figure 7. (upper) Mean annual MLS IWC (mg m^{-3}) at 215 hPa for 2007 (upper left) and the day minus night difference of the IWC values (upper right), where the daytime (nighttime) values come from the ascending (descending) portion of the orbits having local equatorial crossing times of 1:30 pm (am). (lower) Same as upper, except for CloudSat IWC values and for altitude of 11km (~ 215 hPa).

Figure 8. (upper left) Histograms of IWC values from CloudSat, two periods for MLS and two versions of the ECMWF analysis system (R30 and R31) for the periods 08/2006, 08/2005-07/2006, 08/2006, 08/2005-07/2006 and 07/2006, respectively. The MLS and solid-line CloudSat values are based on raw footprints. The dashed-line CloudSat values is based on data first aggregated to $1^{o}x1^{o}$ grid boxes. (upper right) CloudSat and ECMWF values shown are same as left panel, additions are for GEOS5 (1/2006), and NASA fvMMFs for the periods 07/1998, where the latter includes values of graupel, snow, cloud and total ice.

Figure 9. Annual and zonal mean values of cloud ice water content (IWC; mg m^{-3}) from NCAR CAM3 (upper left; 1979-1999), NASA GEOS5 (middle left; 01/1999-12/2002), ECMWF R30 analysis (lower left; 08/2005-07/2006), fvMMF (upper right, 07/98 & 01/99), and RAVE GCM (middle right; 1998).

Figure 10. Annual mean values of graupel (upper left), cloud ice (middle left), snow (lower left) and their sum (upper right) from the RAVE GCM, along with their zonal mean values (lower right) and percent contribution of each of the constituents to the total ice (middle right) [black = total, red = snow, graupel = blue, cloud = green].

Figure 11. Annual mean values of graupel (upper left), cloud ice (middle left), snow (lower left) and their sum (upper right) from the NASA fvMMF GCM, along with their zonal mean values (lower right) and percent contribution of each of the constituents to the total ice (middle right) [black = total, red = snow, graupel = blue, cloud = green].

Figure 12. Annual and zonal mean values of graupel (upper), cloud ice (upper middle), snow (lower middle) and their sum (lower) from the RAVE (left) and NASA fvMMF (right) GCMs. Dotted line in lower panel at 300 hPa is for comparison purposes to **Figure 5**.

Figure 13. Annual and zonal mean values of CloudSat IWC (mg m^{-3}) when considering clear cases and those with IWC > 0 but flagged as having no precipitation *at the surface* (NP; upper), cases flagged as non-convective clouds (NC; middle), and those cases that meet both these criteria (NP & NC; lower). Right panels are the same, except for different plotting format for comparison to MLS inset panel in upper right of **Figure 5**. Lower left panel gives the frequency of occurrence of the given IWC > 0 condition, NC (red), NP (blue), and NP & NC (green) relative to all (clear and IWC > 0) cases.

Figure 14. (upper) Mean annual IWP (gm m^{-2}) for CloudSat values flagged as both Non-Precipitating (NP) and Non-Convective (NC) (8/2006-7/2007). (lower) Same, except with color scale matching **Figure 3**.

Figure 15. Mean annual IWC (mg m^{-3}) at 215 hPa for MLS (upper left; 8/2004-7/2006), CloudSat values flagged as both Non-Precipitating (NP) and Non-Convective (NC) (upper right; 8/2006-7/2007), GEOS5 (middle left; 1/1999-12/2002), ECMWF analysis R30 (middle right; 8/2005-7/2006), and NCAR CAM3 (lower left; 1979-1999).

Figure 16. Mean May-July 2006 IWC (mg m^{-3}) at 215 hPa for ECMWF analysis R30 (upper left), R31 (upper right), the relative percent change ((R31 - R30)/R31*100), and the overlapping MLS values (lower right).

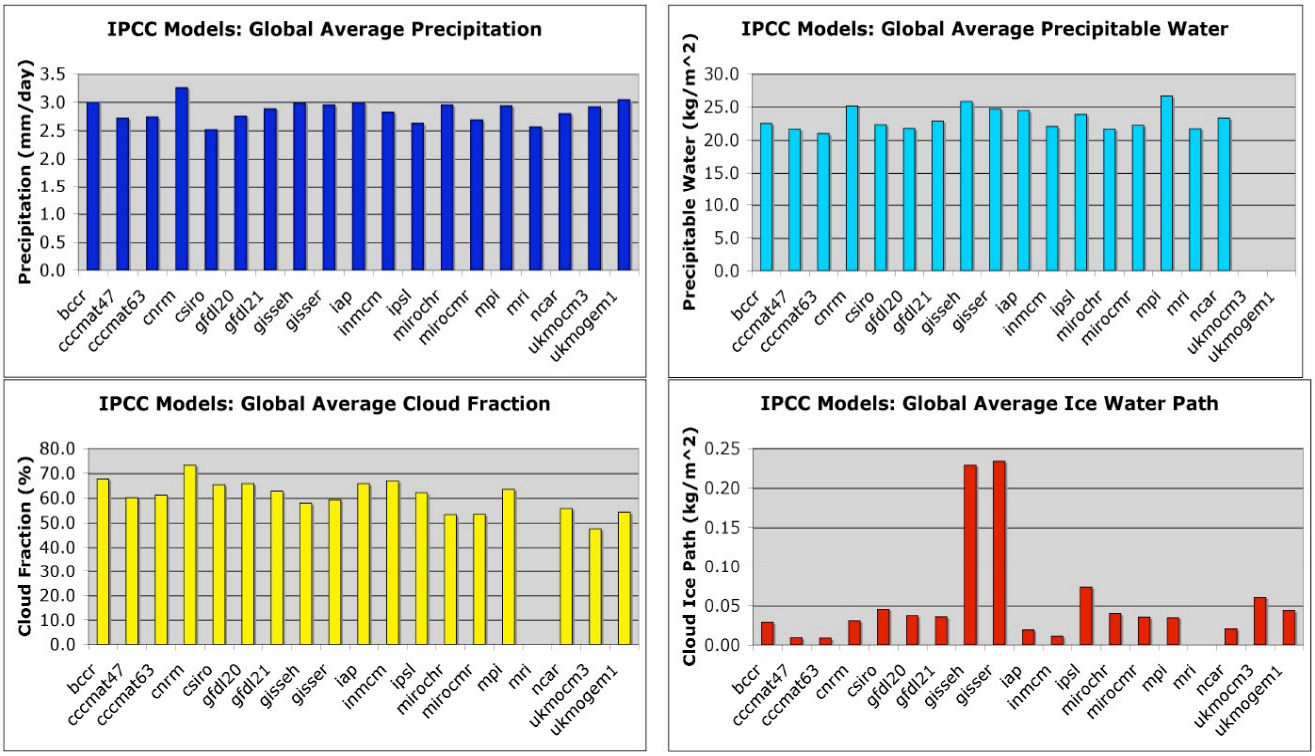

Figure 1. Globally-averaged, annual mean values of precipitation (upper left), precipitable water (upper right), total cloud fraction (lower left) and cloud ice water path (lower right) from the 1970-1994 period of the 20th century GCM simulations contributed to the IPCC 4th Assessment Report (20c3m scenario). Zero values indicate that the given model did not provide this variable to the IPCC database.

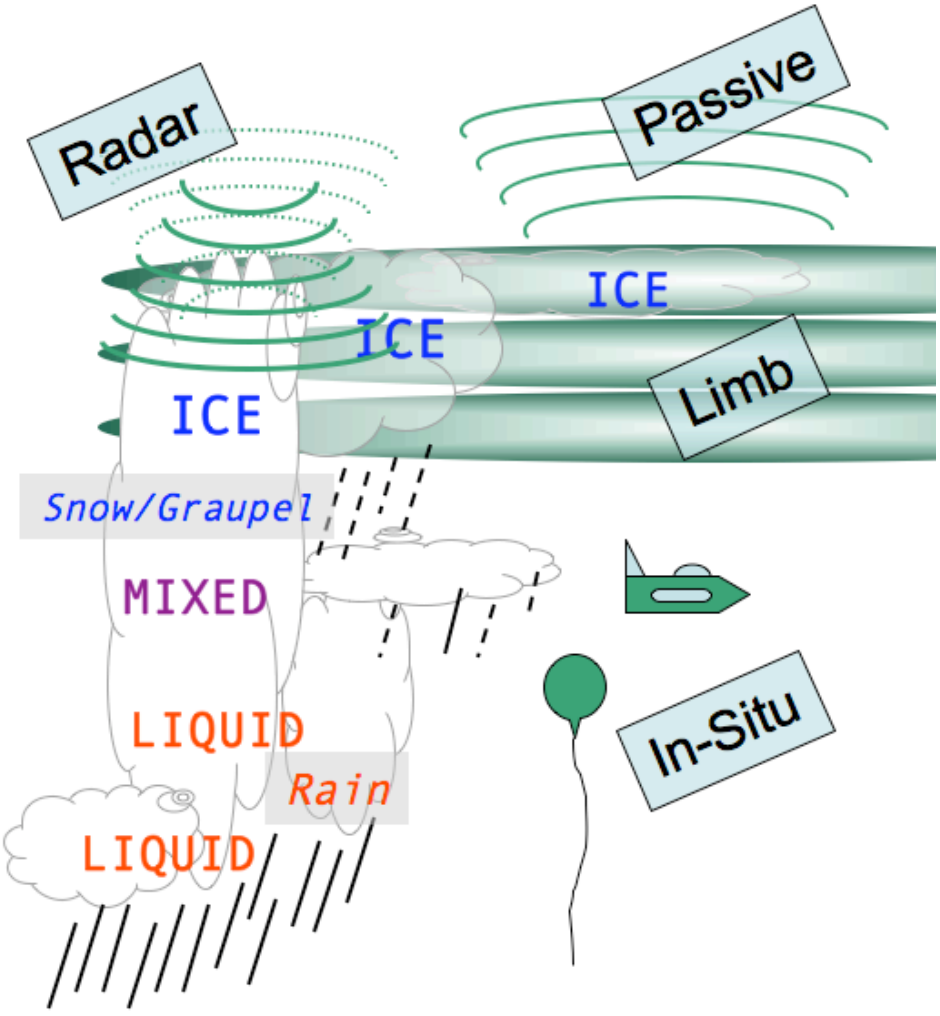

Figure 2. Schematic diagram illustrating measurement methods for estimating cloud ice water content/path, including in-situ measurements as well as passive, radar and limb-sounding satellite techniques.

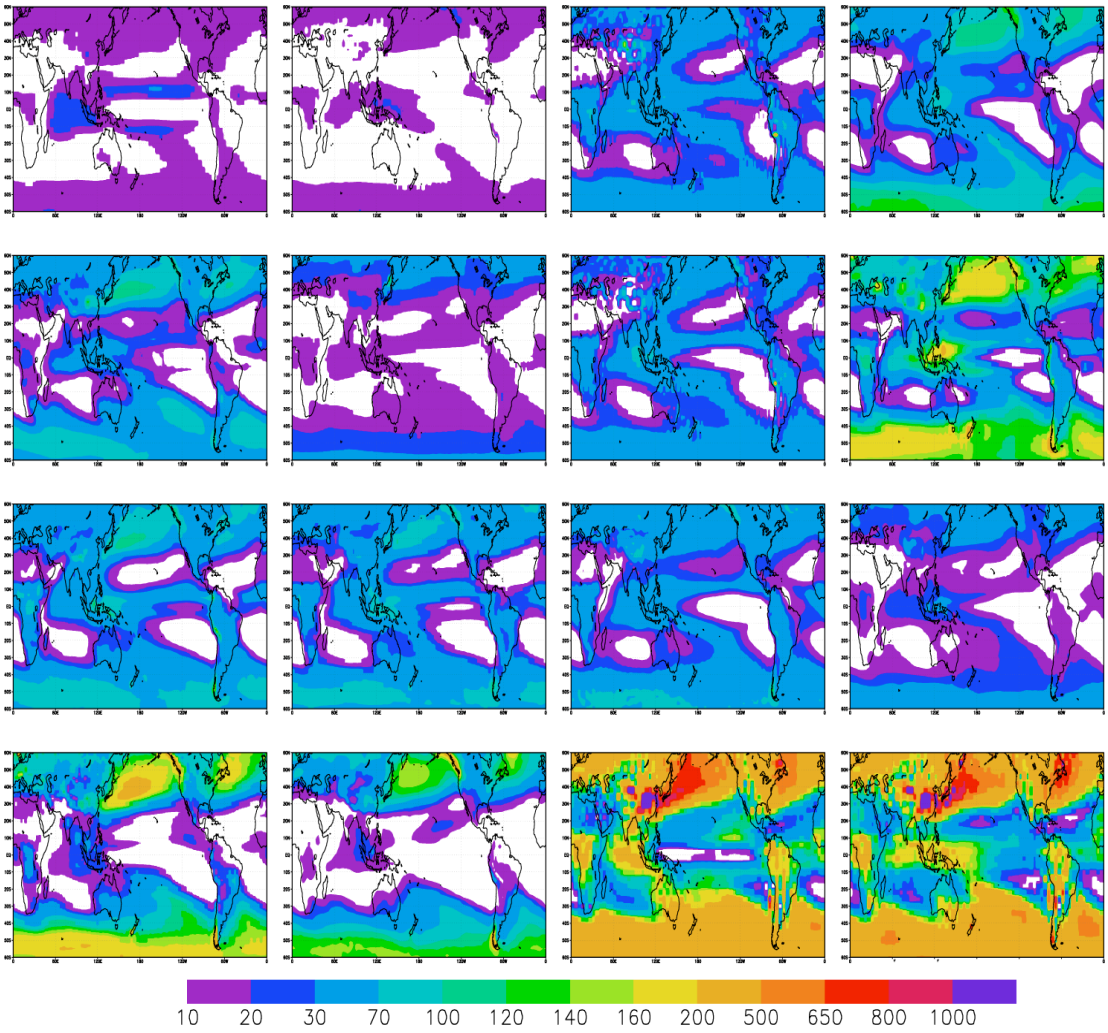

Figure 3. Annual mean values of cloud ice water path (IWP; gm m^{-2}) from the 1970-1994 period of the 20th century GCM simulations contributed to the IPCC 4th Assessment Report (20c3m scenario); Note that the color scale is not linear.

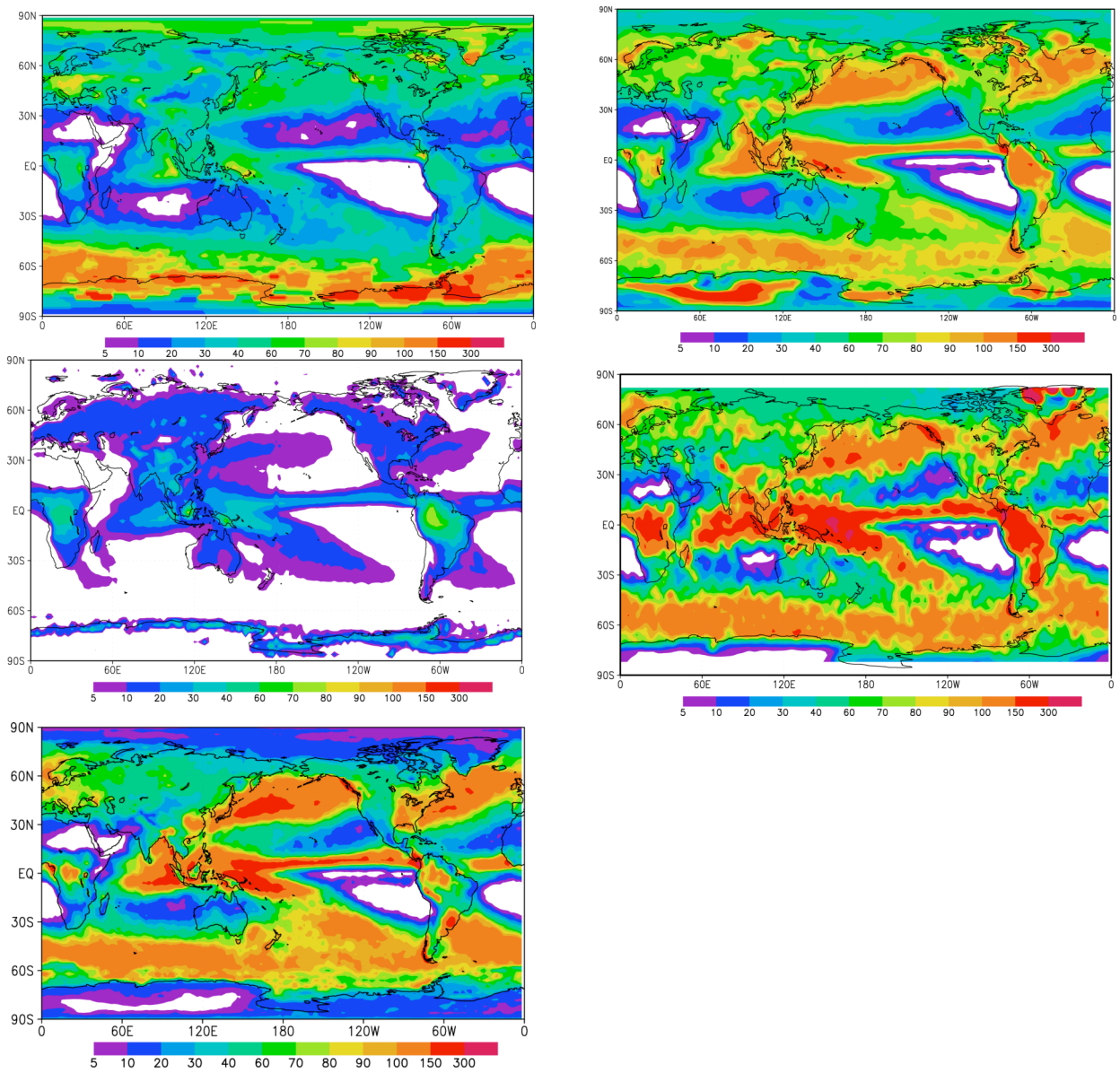

Figure 4. Annual mean values of cloud ice water path (IWP; gm m^{-2}) from ISCCP (upper left; 2005), NOAA/NESDIS (middle left; 2000-2006), CERES/MODIS (lower left; 2001-2005), MODIS MYD06 (upper right; 7/2002-6/2007), and CloudSat (middle right; 8/2006-7/2007). See text for details. Note that the color scale differs from that in Figure 3.

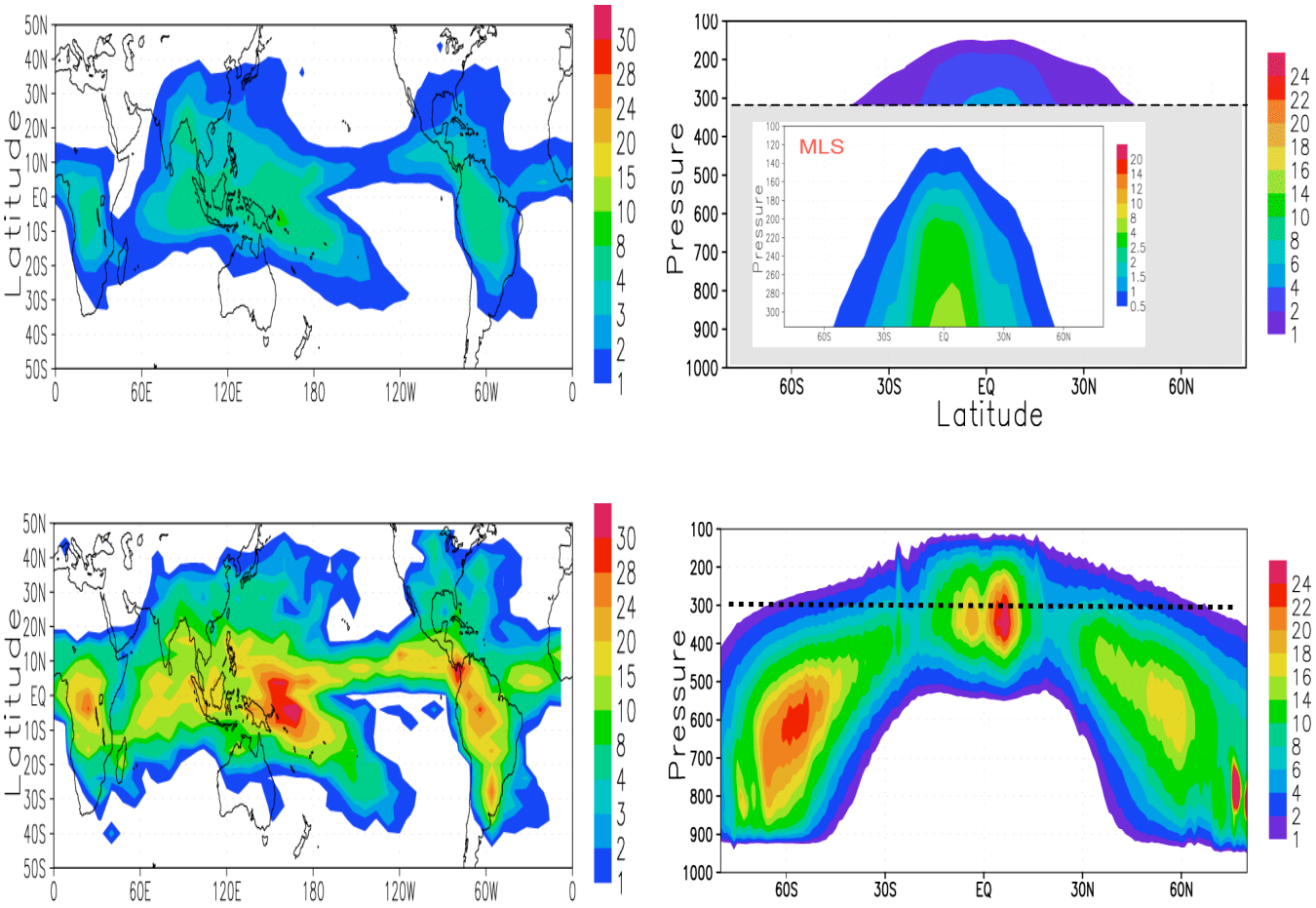

Figure 5. Annual mean values of cloud ice water content (IWC; mg m^{-3}) at 215 hPa (left) and zonal average (right). Values from MLS (upper) are from 8/2004-7/2006, and those from CloudSat (lower) are from 8/2006-7/2007. For upper right panel, MLS retrievals only extend down to 316 hPa (dotted line); inset shows same MLS data as larger panel but with different color scale. Note that MLS data below 215 hPa for this version (1.5) is not part of the official release and was processed offline as an experimental product.

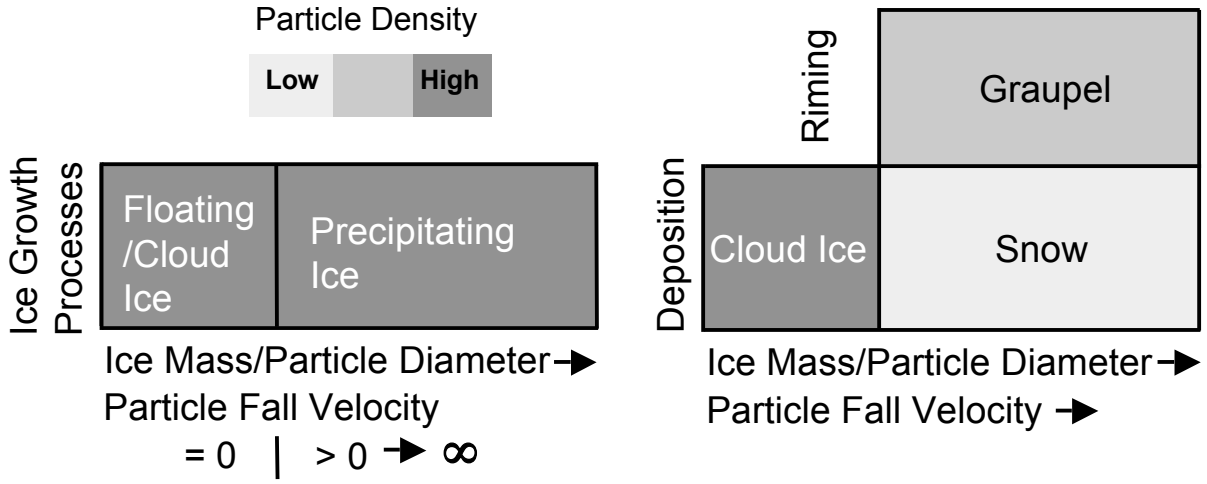

Figure 6. Schematic diagram illustrating basic features of model parameterizations of cloud-related ice for a conventional GCM using a single species microphysics scheme (left) and a 3-species microphysics scheme (right). The vertical axes are associated with ice growth processes and the horizontal axes are associated with ice mass and/or particle diameter and also particle fall velocity. On the left figure, ice growth processes are not distinguished and are all embedded within the simplified parameterization. On the right figure, deposition is the primary process associated with cloud and snow, while riming is the primary processes responsible for graupel formation. On the left figure, cloud ice is assumed to be floating, i.e. zero fall velocity, and the ice deemed to be precipitating is removed immediately, i.e. infinite fall velocity. Shading is an indication of the density of particles.

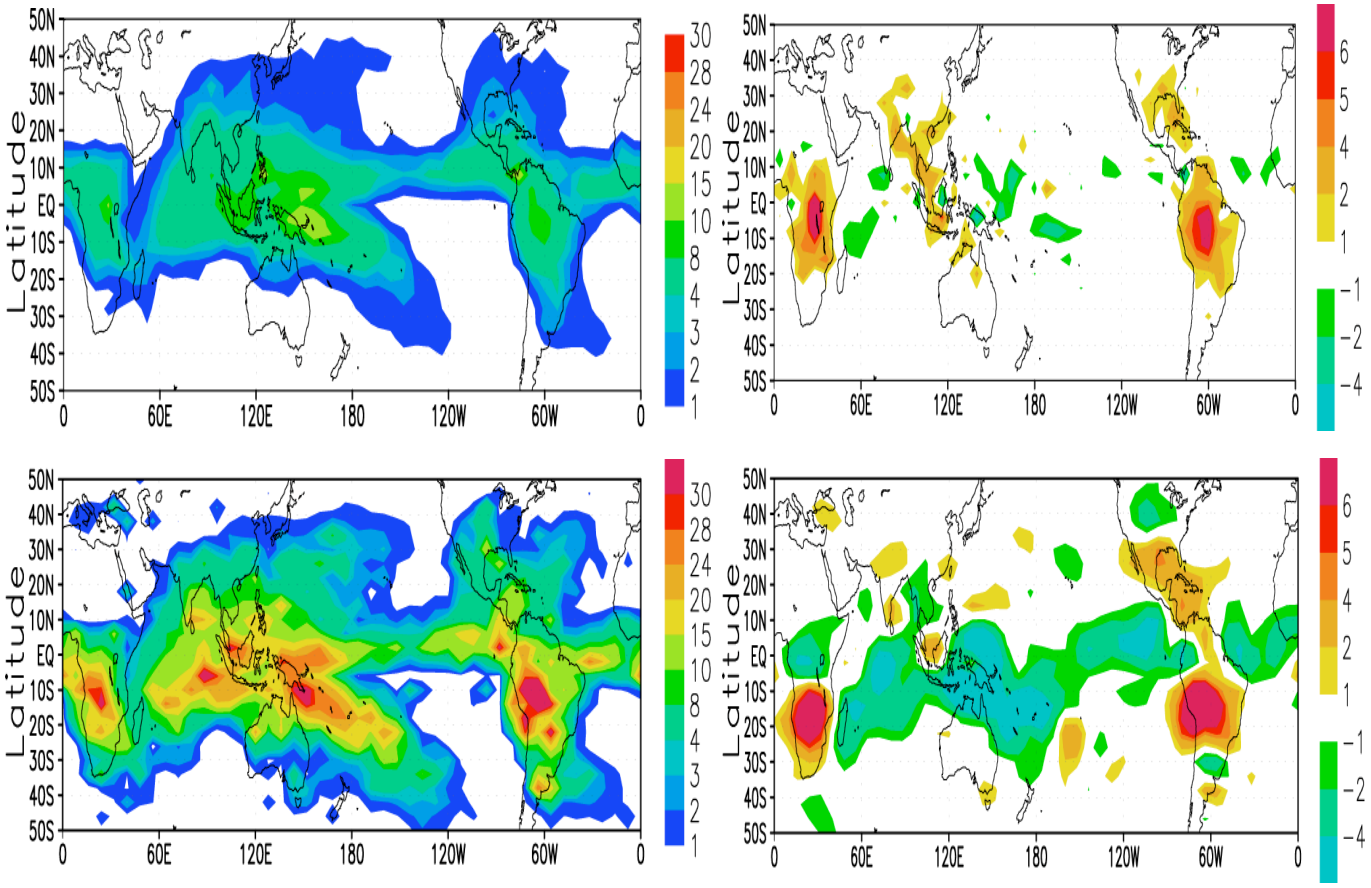

Figure 7. (upper) Mean annual MLS IWC (mg m^{-3}; Version 2.2) at 215 hPa for 2007 (upper left) and the day minus night difference of the IWC values (upper right), where the daytime (nighttime) values come from the ascending (descending) portion of the orbits having local equatorial crossing times of 1:30 pm (am). (lower) Same as upper, except for CloudSat IWC values for 2007 and for altitude of 11km (~ 215 hPa).

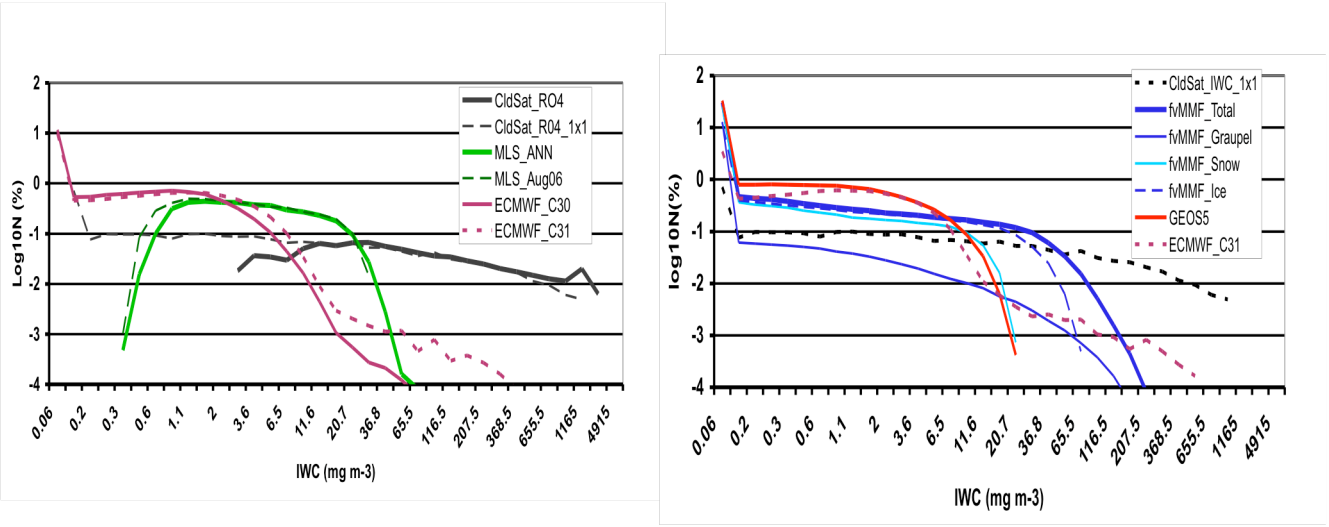

Figure 8. (upper left) Histograms of IWC values from CloudSat, two periods for MLS and two versions of the ECMWF analysis system (R30 and R31) for the periods 08/2006, 08/2005-07/2006, 08/2006, 08/2005-07/2006 and 07/2006,, respectively. The MLS and solid-line CloudSat values are based on raw footprints. The dashed-line CloudSat values is based on data first aggregated to 1°x1° grid boxes. (upper right) CloudSat and ECMWF values shown are same as left panel, additions are for GEOS5 (1/2006), and NASA fvMMFs for the periods 07/1998, where the latter includes values of graupel, snow, cloud and total ice.

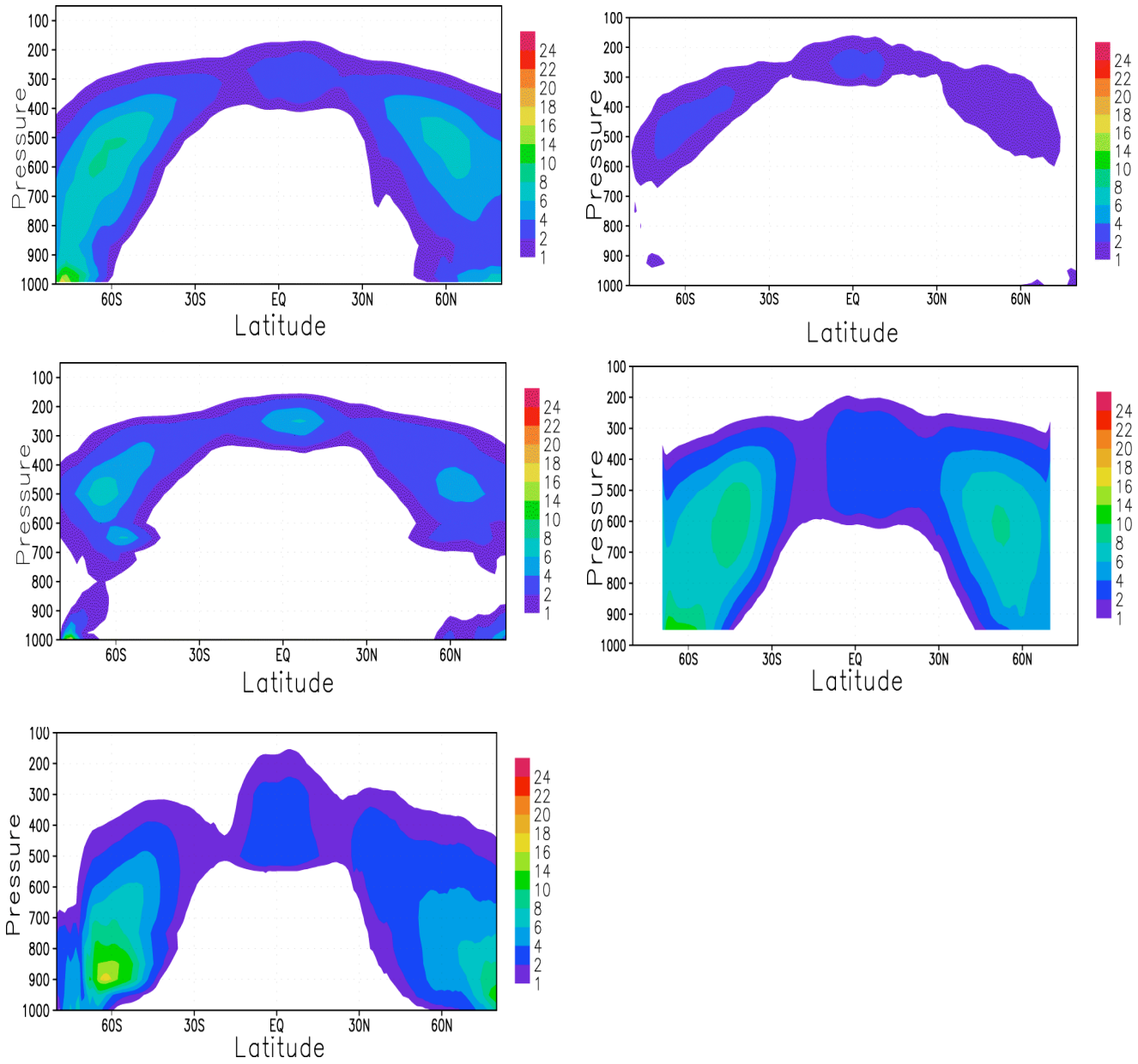

Figure 9. Annual and zonal mean values of cloud ice water content (IWC; mg m^{-3}) from NCAR CAM3 (upper left; 1979-1999), NASA GEOS5 (middle left; 01/1999-12/2002), ECMWF R30 analysis (lower left; 08/2005-07/2006), fvMMF (upper right, 07/98 & 01/99), and RAVE GCM (middle right; 1998).

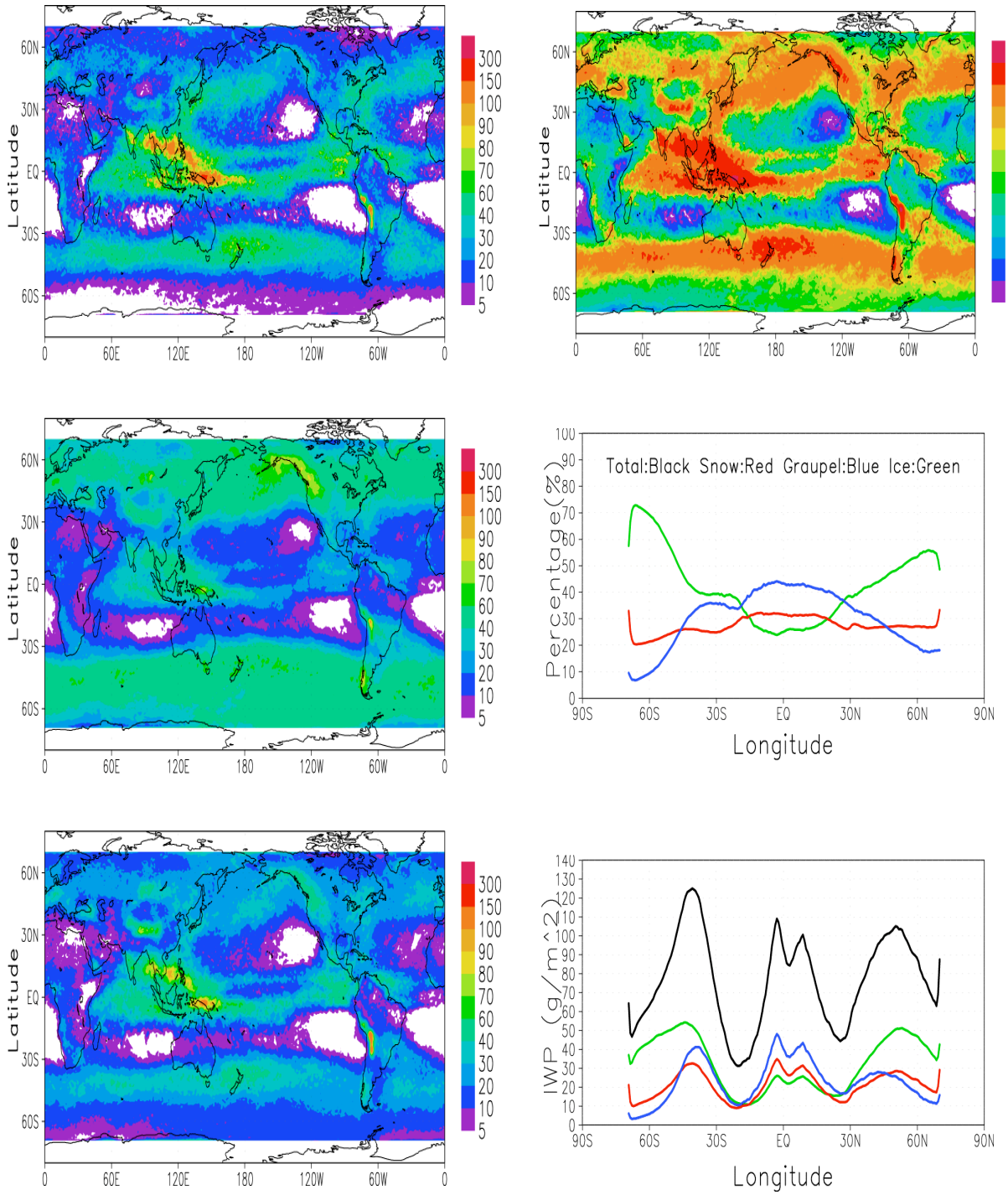

Figure 10. Annual mean values of IWP (gm m^{-2}) for graupel (upper left), cloud ice (middle left), snow (lower left) and their sum (upper right) from the RAVE GCM, along with their zonal mean values (lower right) and percent contribution of each of the constituents to the total ice (middle right) [black = total, red = snow, graupel = blue, cloud = green].

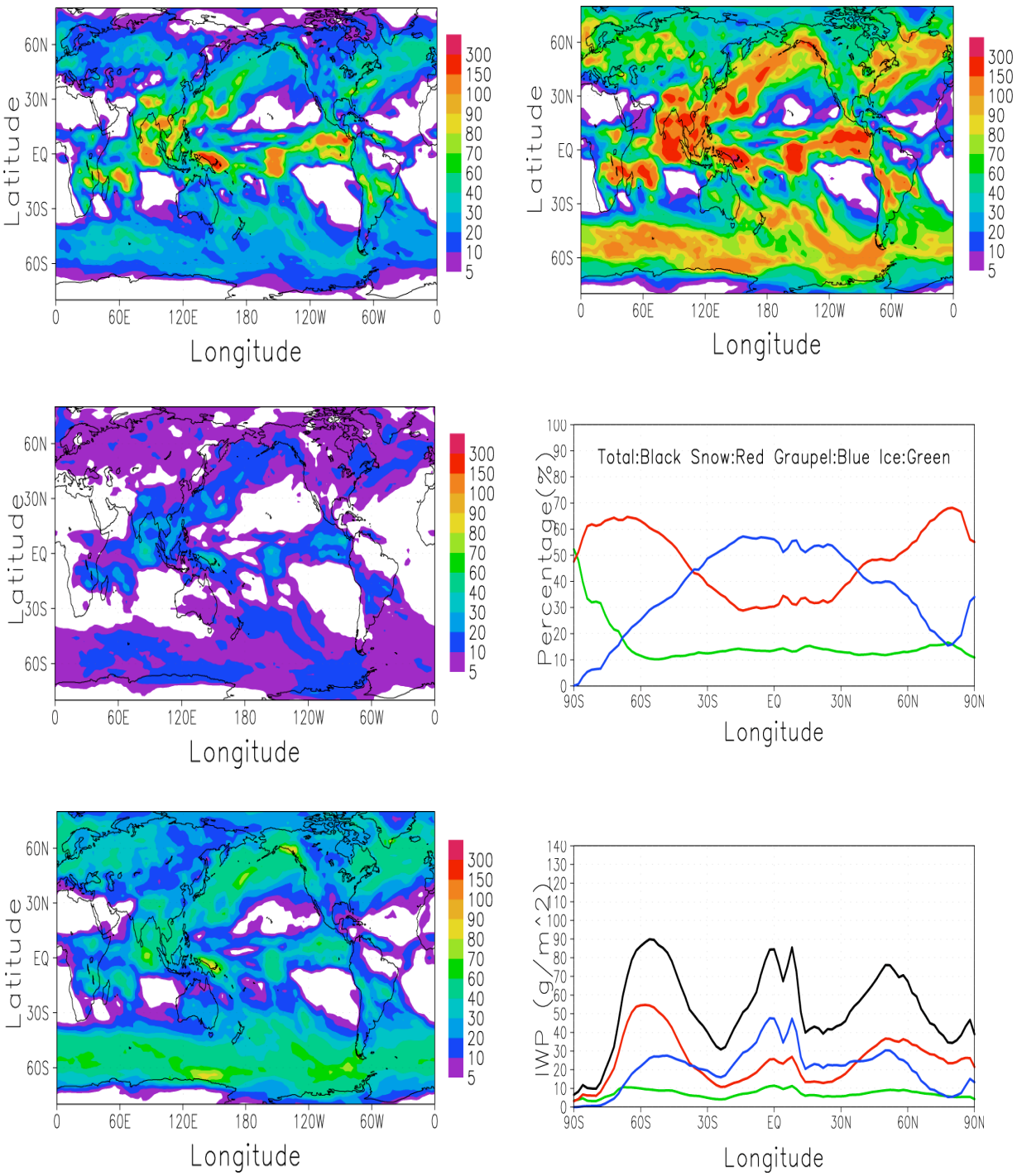

Figure 11. Annual mean values of IWP (gm m^{-2}) for graupel (upper left), cloud ice (middle left), snow (lower left) and their sum (upper right) from the NASA fvMMF GCM, along with their zonal mean values (lower right) and percent contribution of each of the constituents to the total ice (middle right) [black = total, red = snow, graupel = blue, cloud = green].

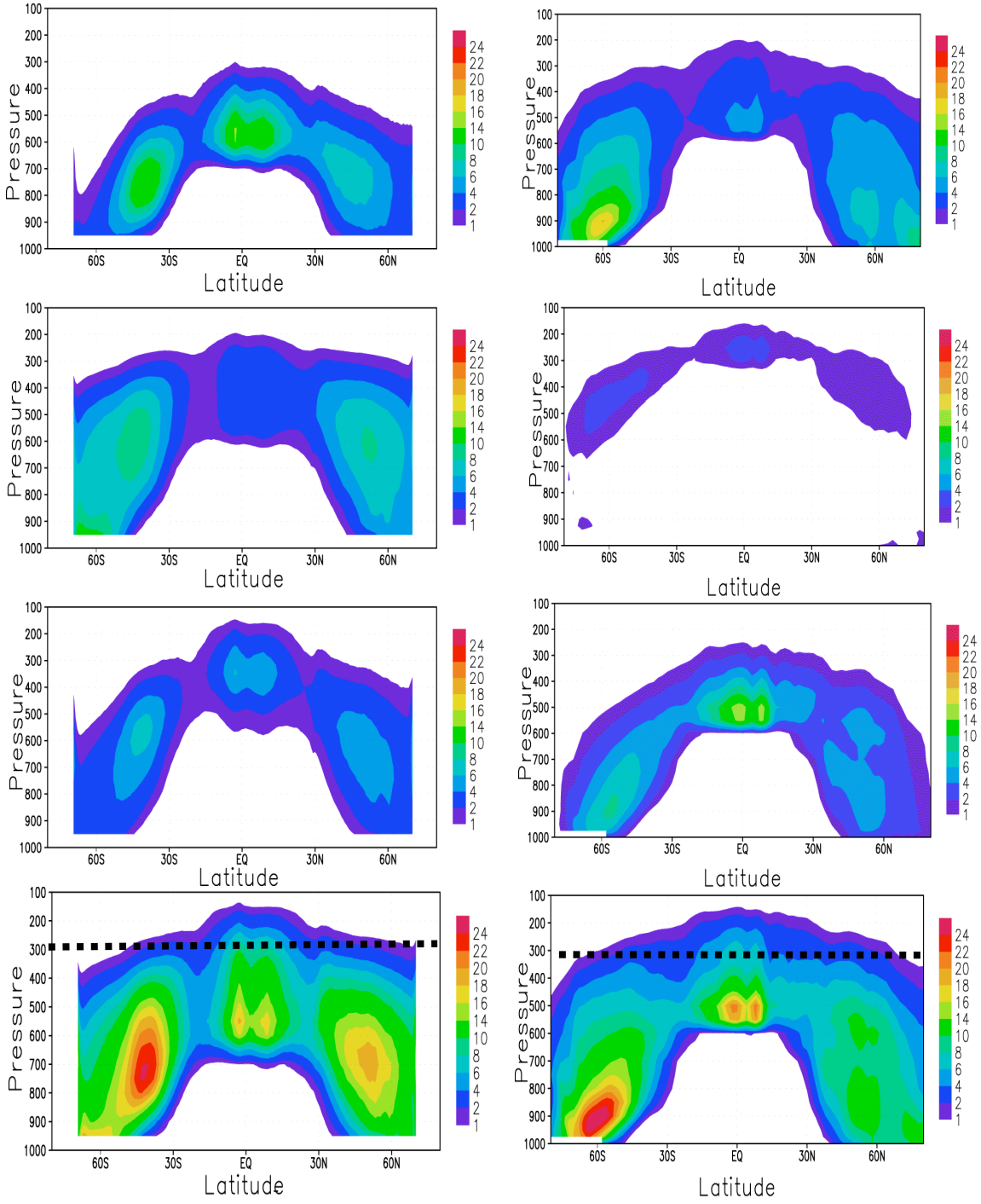

Figure 12. Annual and zonal mean values of of IWC (mg m^{-3}) for graupel (upper), cloud ice (upper middle), snow (lower middle) and their sum (lower) from the RAVE (left) and NASA fvMMF (right) GCMs. Dotted line in lower panel at 300 hPa is for comparison purposes to Figure 5.

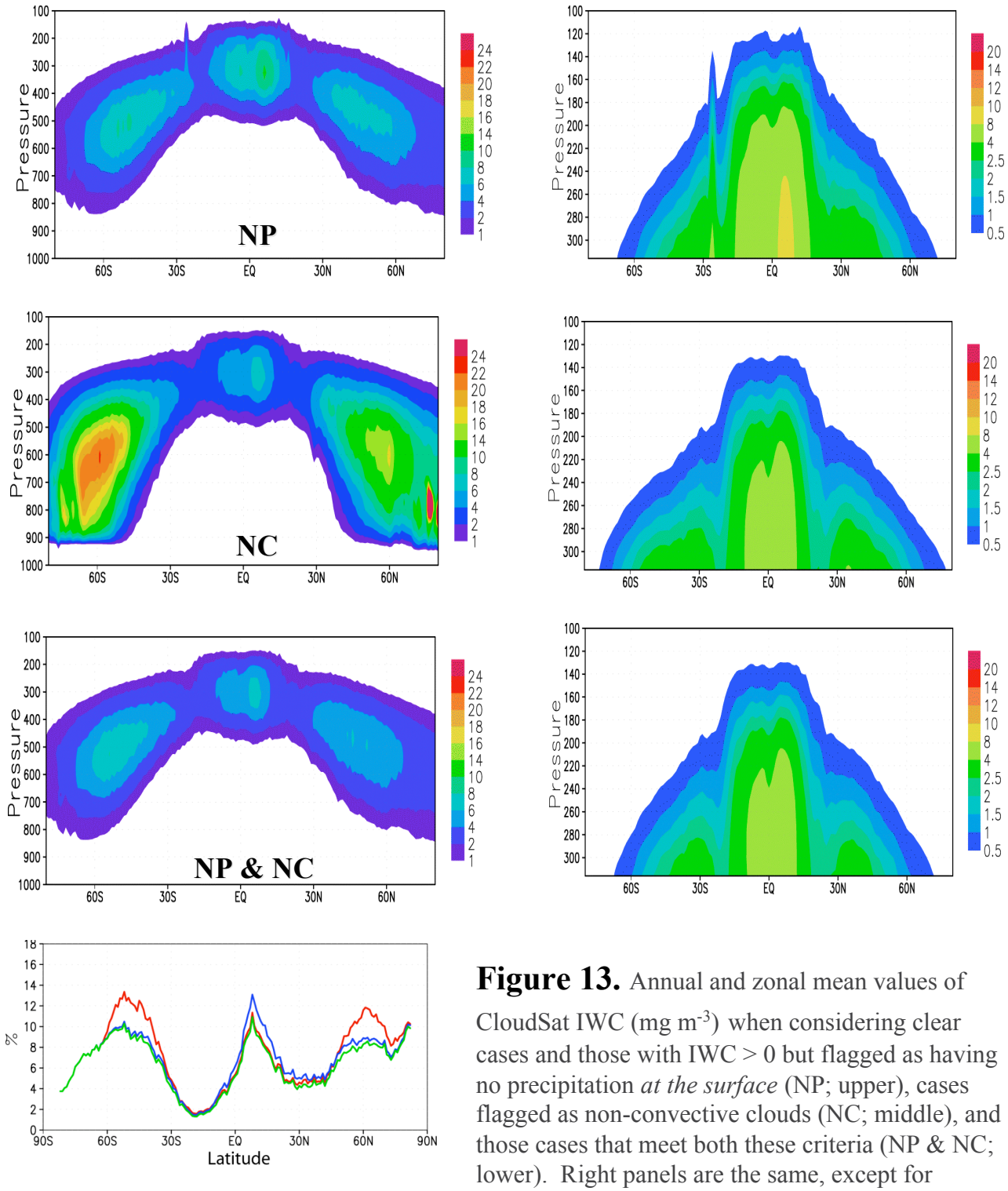

Figure 13. Annual and zonal mean values of CloudSat IWC (mg m^{-3}) when considering clear cases and those with IWC > 0 but flagged as having no precipitation *at the surface* (NP; upper), cases flagged as non-convective clouds (NC; middle), and those cases that meet both these criteria (NP & NC; lower). Right panels are the same, except for different plotting format for comparison to MLS inset panel in upper right of Figure 5. Lower left panel gives the frequency of occurrence of the given IWC > 0 condition, NC (red), NP (blue), and NP & NC (green) relative to all (clear and IWC > 0) cases.

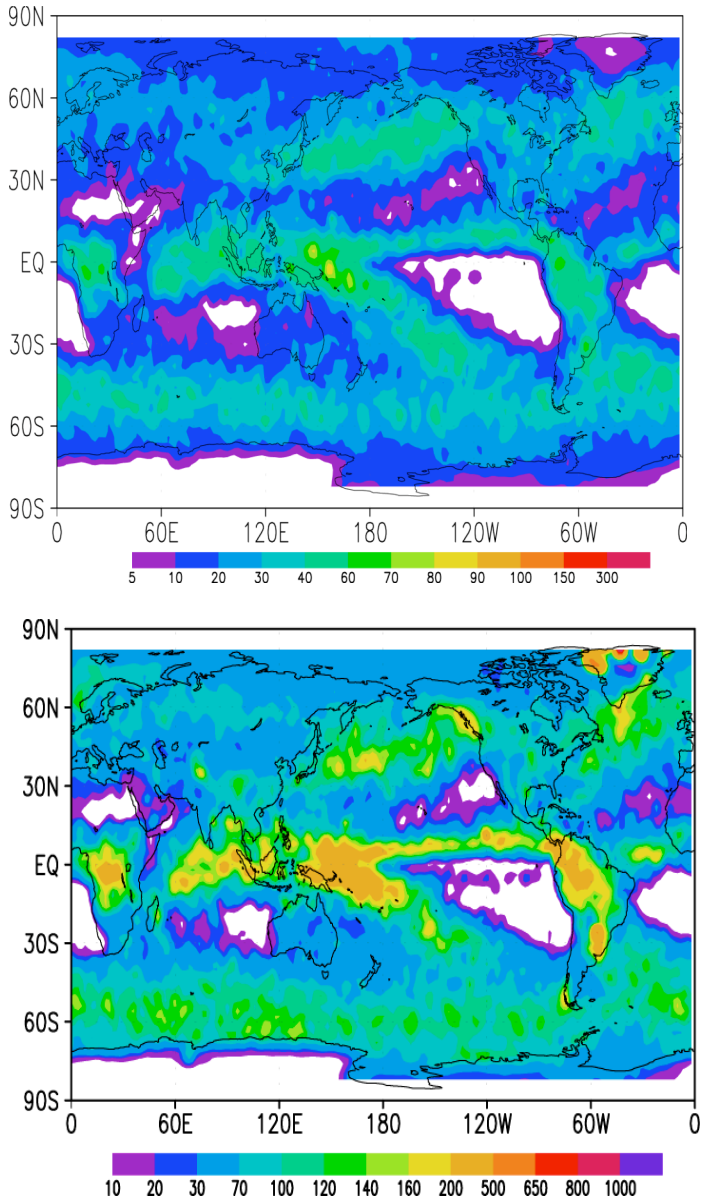

Figure 14. (upper) Mean annual IWP (gm m^{-2}) for CloudSat values flagged as both Non-Precipitating (NP) and Non-Convective (NC) (8/2006-7/2007). (lower) Same, except with color scale matching Figure 3.

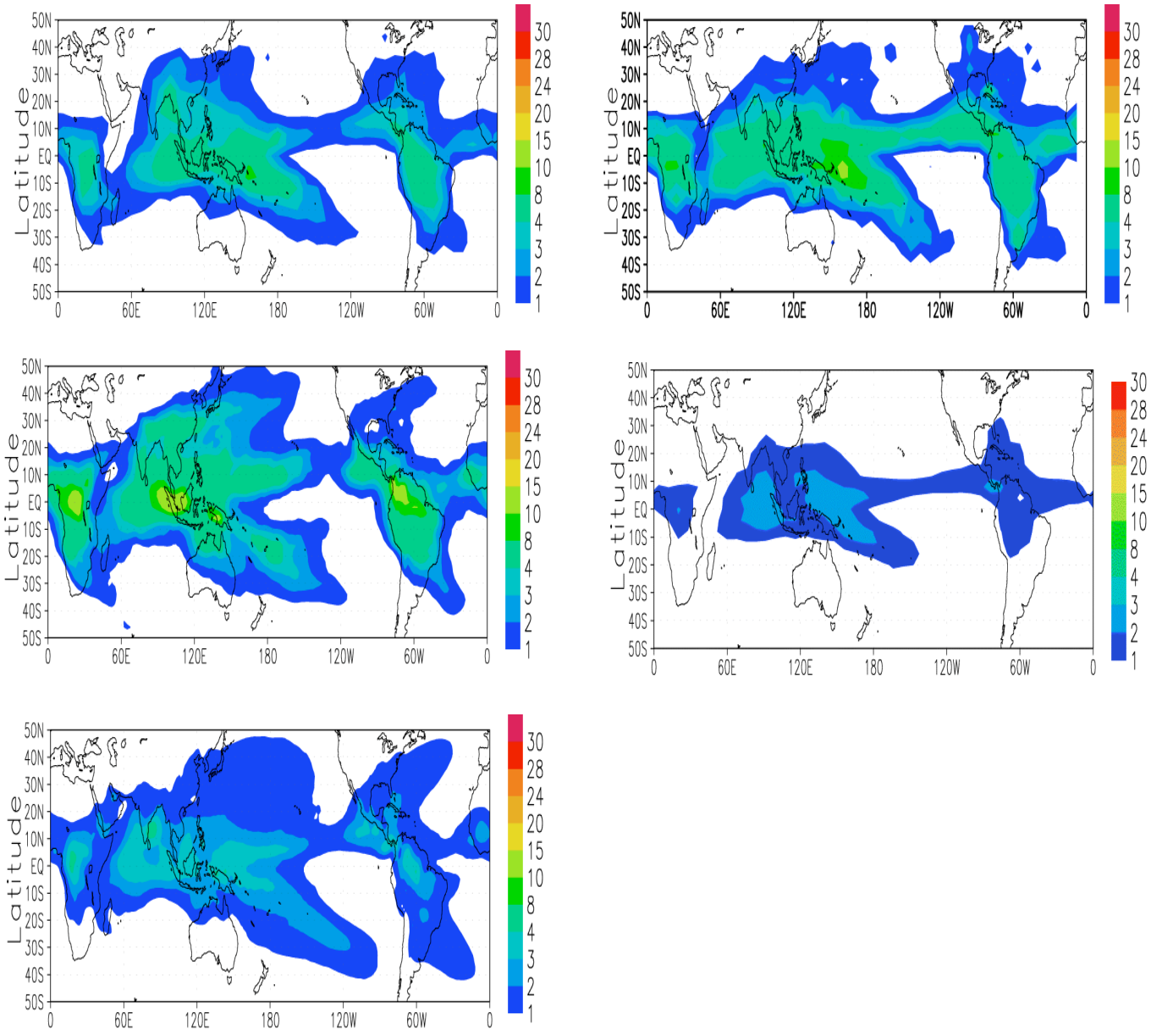

Figure 15. Mean annual IWC (mg m^{-3}) at 215 hPa for MLS (upper left; 8/2004-7/2006), CloudSat values flagged as both Non-Precipitating (NP) and Non-Convective (NC) (upper right; 8/2006-7/2007), GEOS5 (middle left; 1/1999-12/2002), ECMWF analysis R30 (middle right; 8/2005-7/2006), and NCAR CAM3 (lower left; 1979-1999).

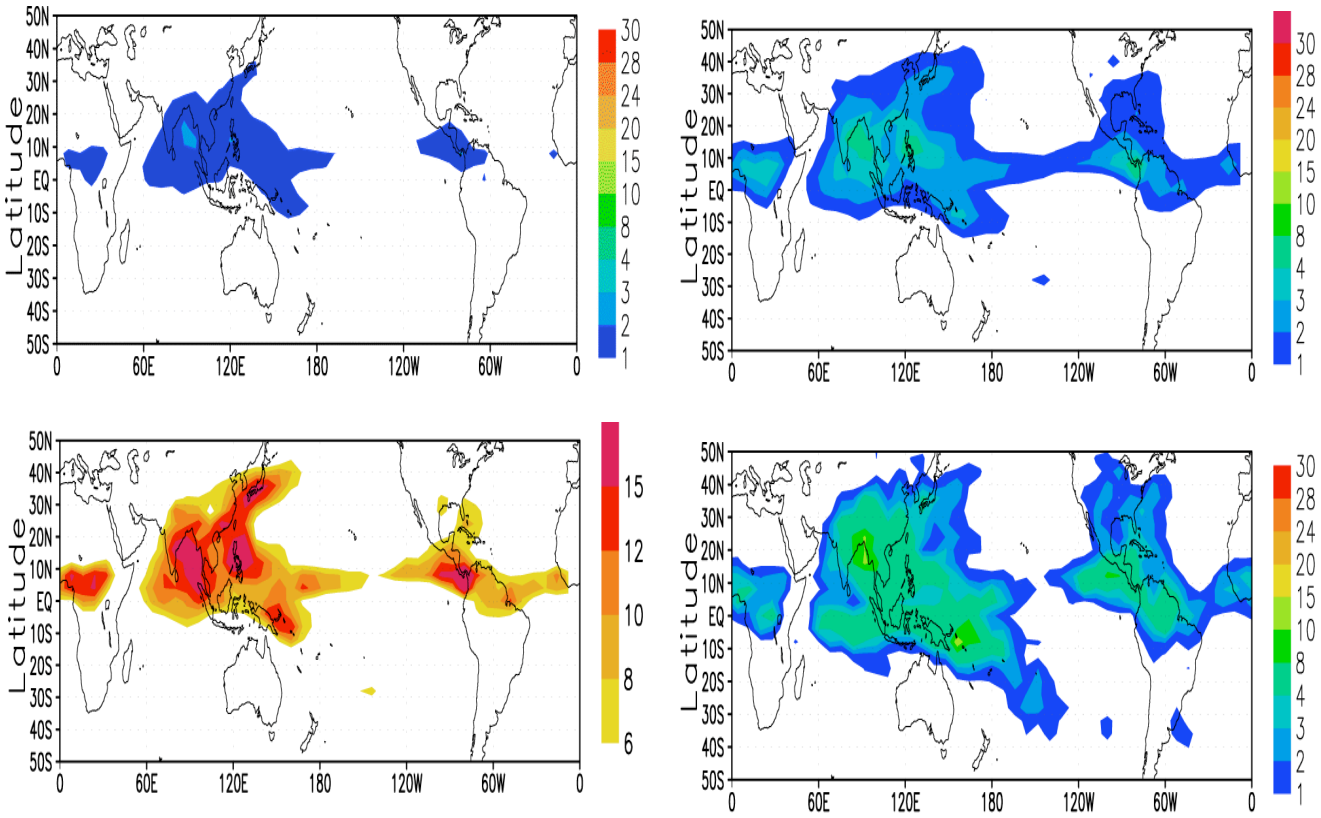

Figure 16. Mean May-July 2006 IWC (mg m^{-3}) at 215 hPa for ECMWF analysis R30 (upper left), R31 (upper right), the relative percent change ((R31 - R30)/R31*100), and the overlapping MLS values (lower right).